AD 262 743

AEDC-TN-61-106

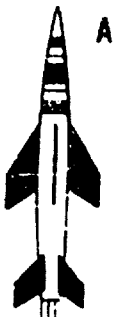

AN INVESTIGATION OF BASE HEATING ON A 5.47-PERCENT SCALE MODEL OF THE SATURN S-1 BOOSTER AT TRANSONIC MACH NUMBERS

By

T. L. Kennedy and J. F. Lowry
PWT, ARO, Inc.

August 1961

ARNOLD ENGINEERING DEVELOPMENT CENTER

AIR FORCE SYSTEMS COMMAND

U S A F

AN INVESTIGATION OF BASE HEATING ON A 5.47-PERCENT SCALE MODEL OF THE SATURN S-1 BOOSTER AT TRANSONIC MACH NUMBERS

By

T. L. Kennedy and J. F. Lowry
PWT, ARO, Inc.

August 1961

AFSC Program Area 921E, Project 9018
ARO Project No. 224164

Contract No. AF 40(600)-800 S/A 24(61-73)

ABSTRACT

An investigation was conducted in the 16-Ft Transonic Tunnel of the Propulsion Wind Tunnel Facility at the Arnold Center to evaluate base heating of the Saturn S-1 Booster.

Various turbine exhaust stack configurations were tested over a Mach number range of 0.6 to 1.5, an altitude range of 10,000 ft to 42,000 ft, and a missile angle-of-attack range of 0 to -7 1/2 deg. Rocket engines using liquid oxygen and RP-1 were used to simulate the full-scale engine exhaust, and hydrogen was used to simulate the turbo-pump exhaust.

Base burning at all test conditions was eliminated for only one of the turbine exhaust stack configurations. Various degrees of base burning were obtained for all other exhaust stack configurations, but no burning occurred at a free-stream Mach number of 1.5 for the trajectory altitude. At altitudes above 29,000 ft, only localized base burning occurred and the accompanying heating rates were low.

CONTENTS

TABLE

ILLUSTRATIONS

NOMENCLATURE

c_p	Specific heat of calorimeter slug (function of material and temperature), Btu/lb-°R
D	Body diameter, 13.92 in.
$\frac{dT}{dt}$	Slope of temperature-time history curve
h_c	Experimental convection film conductance, $\frac{dq}{dT}$, Btu/ft^2-sec-°R
M_∞	Free-stream Mach number
M_x	Local Mach number
O/F	Oxidizer to fuel weight flow ratio
p_∞	Free-stream static pressure, lb/ft^2
p_b	Average base static pressure, lb/ft^2
q	Calorimeter heating rate, $\rho c_p \frac{dT}{dt}$, Btu/ft^2-sec
Δq	Change in calorimeter total heat rate due to turbine exhaust introduction, Btu/ft^2-sec ($q_{\text{turbine exhaust on}} - q_{\text{turbine exhaust off}}$)
T	Temperature °F
T_g	Gas temperature, °F
$(T)_{q=0}$	Estimated equilibrium temperature, °F
t	Time, sec
x	Distance from model surface, in.
α	Model angle of attack, deg
θ	Calorimeter location, deg clockwise around an engine (The line connecting the center of the engine and the center of its turbine exhaust duct is zero deg.)
ρ	Density of slug material, lb/ft^3
τ	Thickness of calorimeter slug, ft

INTRODUCTION

At the request of the George C. Marshall Space Flight Center, NASA, tests were conducted to determine base heating on a 5.47-percent scale model of the Saturn S-1 booster. Reported herein are the results of tests conducted in the 16-Ft Transonic Tunnel of the PWT, Arnold Center, Air Force Systems Command, from May 9 to May 26, 1961.

Scale rocket engines burning liquid oxygen and RP-1 were used to produce the main engine exhaust. Hydrogen was used to simulate the fuel-rich turbo-pump exhaust. Several exhaust stack configurations were tested covering a Mach number range from 0.6 to 1.5 at predicted trajectory altitudes. In addition, more extensive tests were made with one turbine exhaust configuration to determine the effects of angle of attack, one-engine inoperative, and off-trajectory altitudes on base-heating.

APPARATUS

TEST FACILITY

The PWT 16-Ft Transonic Tunnel is a continuous flow, closed-circuit type wind tunnel in which Mach number can be varied from 0.5 to 1.6 and altitude from sea level to over 100,000 ft. The rocket exhaust gases are removed from the circuit by scavenging system, and simultaneously, conditioned air is supplied through the make-up air system to maintain the tunnel at equilibrium conditions. More complete descriptions of the tunnel and propulsion testing therein are given in Refs. 1 and 2, respectively. Shown in Fig. 1 is a sketch of the tunnel test section with the basic model installed.

The rocket propellant system includes equipment designed to deliver liquid oxygen and fuel at controlled flow rates and auxiliary systems providing for engine ignition, water cooling, and nitrogen for line purging and shroud line pressurization. The rocket propellant system is shown schematically in Fig. 2, and a more complete description of the system is given in Ref. 3.

Manuscript released by authors August 1961.

TEST ARTICLE

An arbitrary forebody was used with an exact scale shroud and engine compartment. The model had a spherical nose section and a conic transition to the cylindrical body. The contoured aft section was fitted with eight engines and a removable heat shield. Views of the strut mounted model in the 16-Ft test section are shown in Fig. 3. A dimensional sketch of the model is shown in Fig. 4.

Turbo-Pump Exhausts

The simulated turbo-pump exhaust for the four outer engines was ducted through exhausterators installed on each of the engines. The design was such that the exhaust was injected into the jet at 90 deg to the jet through an annular slot at the jet exit plane.

Various exhaust stack configurations which projected from the side of the model were used to simulate turbo-pump exhaust ducts for the four inner engines. The exhaust stack configurations tested are shown in Figs. 5 through 7. The heating value of the exhaust of the full-scale turbines was simulated by a flow of approximately 0.01 lb/sec of hydrogen through each of the eight turbine exhausts.

Engines

The rocket engines which were developed by the George C. Marshall Space Flight Center, NASA, has an area ratio of 7.72 and were designed to operate at a nominal chamber pressure of 500 psia, an O/F ratio of approximately 2, and a total propellant flow of 2.25 lb/sec per engine. Cooling was accomplished with an integral water jacket at a flow rate of 3 lb/sec. All engines were ignited simultaneously by injecting triethylaluminum (a pyrophoric fuel) into a section of a secondary fuel line. Injection of the pyrophoric fuel into the engine by the secondary fuel flow resulted in ignition with LO_2 and subsequent burning of the secondary flow which was followed by the main stage fuel flow. The triethylaluminum and subsequent secondary fuel flow entered at the center of the injector, and the main stage fuel was introduced through peripheral rows of orifices in the injector.

INSTRUMENTATION

Calorimeter and pressure orifice locations on the heat shield are shown in Fig. 8. During engine operation, heat shield temperatures and pressure measurements were continuously commutated at a rate of

100 per second into a high-speed digitizer and recorded on magnetic tape. Base pressure transducers were located in the model, and calorimeter temperatures were measured by means of chromel alumel thermocouples.

CALORIMETERS

The model heat shield was of sandwich construction and consisted of a 1/16-in. thick mild steel forward plate and a 1/16-in. thick copper aft plate. The segments were separated with a 0.38-in. thick sheet of MIN-K insulating material. The calorimeters were mounted flush with the aft plate. The calorimeter location designations shown in Fig. 8 also indicate the type of calorimeter. Calorimeter descriptions and constants are presented in Table 1 for each type of calorimeter.

ENGINE INSTRUMENTATION

Transducers located in the model measured individual engine chamber pressures, which were monitored on strip chart recorders. These recorders were used also as permissive switches to prevent opening of the main stage fuel valve unless each engine was running on secondary fuel flow. Millivolt indicators were used to monitor engine cooling water temperature rise and also to provide an over-temperature cutoff. Water, liquid oxygen, and RP-1 fuel flow rates were monitored by using turbine-type flow meters.

PROCEDURE

These tests were run at predicted Saturn trajectory altitudes and Mach numbers. Several test points were run to investigate the effect of free-stream static pressure on base heating at a fixed Mach number. Full-scale engine chamber pressure could not be attained with the existing scale engines. In order not to compromise the phenomenon of base burning, correct altitude pressures were run rather than match exit pressure ratio. The turbo-exhaust was simulated with hydrogen at a weight flow which duplicated the scale heating value of the fuel-rich turbo-pump exhaust. The exit total and static pressures and temperature of the full-scale turbine exhaust were not simulated.

In each test run the tunnel conditions were established at the desired Mach number and altitude, and a test point was taken to document the tunnel set conditions. A countdown of 15 seconds was used to

start transient recording equipment and cameras, and a test point to establish the essentially steady-state data was automatically recorded at +5 seconds. Engine operation at stabilized chamber conditions had a duration of 10 seconds. The engines were operated at approximately 500 psia chamber pressure and an O/F ratio of approximately 2.1. No attempt was made to investigate these parameters as test variables. Heating rates with turbine-exhaust off were established during the first four seconds of main stage engine operation; the hydrogen valve was then opened, and heating rates were established with the simulated turbine exhaust flow. Unless a configuration change was required, the test conditions for another point on the trajectory were established and the above procedure was repeated.

RESULTS AND DISCUSSION

BOUNDARY-LAYER SURVEY

To document the flow in the vicinity of the aft end of the missile, boundary layer surveys were made 12 in. upstream of the base shroud exit. The results of these surveys made during a portion of the test are shown in Fig. 9.

BASE HEATING

Heating rates were obtained both with and without simulated turbine exhaust for each rocket firing. All heating rates were computed by determining the change in calorimeter temperature over a 0.4-sec time interval and applying the proper calorimeter constant.

Various compromises were required in the scale model, and therefore, the heating rates presented herein are useful in obtaining trends and for configuration comparisons, but should be used with caution to obtain full-scale heating rates. These compromises included differences in inner engine cant-angle and clearance at the exits, engine-exit to free-stream static-pressure ratio, engine O/F ratio, engine combustion efficiency, and turbine exhaust aerodynamic characteristics. The effect of some of these compromises on the base heating rates will be discussed later.

Star Shield Heating

Heating rates for various trajectory conditions as a function of calorimeter temperature for the star shield (see Fig. 8) are shown in

Figs. 10, 11, 12, and 13 for all turbo-exhaust stack configurations. For each test condition, heating rates were established during the whole period of engine operation; the first five seconds provided heating rates for the turbine-exhaust-off and the remainder of the firing provided heating rates for the combined engine and turbo-exhaust operation.

The experimental film heat transfer coefficients obtained by taking the slope of the heating rate temperature data in Figs. 10, 11, 12, and 13 are presented in Fig. 14 as a function of free-stream static pressure (trajectory Mach number is also indicated). Star shield heating was essentially the same for all exhaust configurations. The equilibrium wall temperature determined by extrapolation of the data to a heating rate of zero is shown in Fig. 15. This temperature is believed to be very nearly the local stagnation temperature since the radiation heating rate observed on other portions of the heat shield was small (no satisfactory radiation heating measurements were obtained on the star shield).

The increase in equilibrium wall temperature (Fig. 15) produced when the turbo-exhaust was introduced indicates that the flow at the center of the base was an aspirating one. The near agreement of the equilibrium temperatures and film coefficients with and without turbo-exhaust flow, obtained at the highest Mach numbers and altitudes, indicates that inner-engine exhaust backflow will predominate at higher altitudes. Since the properties of the gas mixture flowing over the star shield are unknown for both the model and full-scale vehicle prior to backflow, correction of the model heating rates to full-scale would be uncertain. If the full-scale and model engine exhaust properties are known, backflow heating rates could be obtained by proper application of Reynolds and Prandtl numbers to the experimental film coefficient. Correction of the adiabatic wall temperature for the higher exhaust gas temperatures of the full-scale configuration would also be required.

The model inner engine 0-deg cant-angle and smaller than scale clearances between the engines at the exits would cause the transition from aspiration to backflow to occur at a lower pressure ratio than the three-degree outward cant-angle and larger clearance spaces of the full-scale booster. Thus, the backflow and higher heating rates would be delayed to some extent for the full-scale configuration. The considerably lower engine exhaust stagnation temperatures of the model engines in comparison to the full-scale engines, however, result in lower star shield turbine-exhaust-off heating rates. Low model engine combustion efficiency and the lower O/F ratio at which peak efficiency was obtained resulted in an estimated stagnation temperature of 3860°R in comparison to a theoretical stagnation temperature of 5600°R at the full-scale O/F ratio.

Primary Heat Shield

For comparison of turbine exhaust stack configurations and test variables, heating rates at fixed calorimeter temperatures are presented. Since heating rate is a function of the calorimeter (or wall) temperature, all heating rates used for comparison purposes were selected at the same calorimeter temperature. The heating rates presented for turbine-exhaust-off are for an arbitrary calorimeter temperature of approximately 100°F. The change in heating rate that is presented to compare the effect of the turbine exhaust is for a calorimeter temperature of approximately 180°F. The heating rates measured on the primary heat shield were lower, in general, than those measured on the star shield. These heating rates and accompanying temperature changes were too small to obtain accurate film coefficients and equilibrium temperatures.

The heating rates without turbine exhaust for various calorimeters are presented as a function of calorimeter azimuth location about two of the outer engines in Fig. 16. With the exception of the calorimeters located at 10 deg and 125 deg, the general level of the turbine-exhaust-off heating rate is approximately 5 Btu/ft^2/sec. The calorimeters with the lower heating rates were partially shielded by the model skin extension beyond the heat shield, and in addition were subjected to cooling from free-stream air flow inducted through nearby scoops. The radiation heating for all locations and test conditions was approximately 2 Btu/ft^2/sec. Assuming that the radiation is proportional to the fourth power of the engine exhaust stagnation temperature, the full-scale radiation level would be approximately 12 Btu/ft^2/sec. Bare thermocouples located in the model just aft of the heat shield indicated an essentially constant temperature of 200°F. This relatively low gas temperature indicated that a negligible amount of engine exhaust was present in the base. Relatively low equilibrium temperatures would be obtained even with the higher full-scale exhaust stagnation temperatures.

The effect of the simulated turbine exhaust flow on base heating is shown in Figs. 17, 18, 20, and 21 as the change in heating rate, which occurred when the turbine exhaust was turned on. An increase in heating occurred for all test conditions in which any effect of turbine exhaust was observed.

Figures 17 and 18 show a comparison of the base heating for different turbine exhaust configurations at M_∞ = 0.8 and 1.2. The heat flux did not increase above turbine-exhaust-off heating rates at M_∞ = 1.5 for any of the configurations, nor did the turbine exhaust produce any convective cooling in the base. The streamlined exhaust stacks (configuration 3) showed no increase in base heating rate at any test condition. The fact

that base burning was eliminated with this configuration indicates that the exhausterators on the four outboard engines did not cause significant base burning. No significant differences in base heating were observed at M_∞ = 0.8 for the other exhaust stack configurations; however, at M_∞ = 1.2 for configuration 2 (short stack), the heating rate increases were greater than for configuration 1-A (long stack, streamline bracket). The heating rates measured around engine number 2 location were significantly higher than for the engine number 3 location when the short stacks were used. This may be attributed to differences in stack height (the stack height in this quadrant was 12 percent lower than in the others).

Insufficient thermocouple instrumentation was installed to determine gas temperature profiles in the boundary layer or temperature distributions at the surface of the heat shield. Thermocouples projecting through the primary heat shield near engine number 3 (see Fig. 8) however, had a very rapid response and measured essentially constant temperatures during each of the phases of operation (turbine-exhaust-off and turbine-exhaust-on). A qualitative comparison of the base burning for the turbine exhaust stack configurations was, therefore, readily obtained from these temperatures as shown in Fig. 19. The conclusions drawn from these comparisons are the same as those obtained from the heating rates. The temperatures indicate no base burning with configuration 3 and configuration 2, compared to 1-A, showed increased burning at M_∞ = 1.2 and reduced burning at M_∞ = 0.8. No burning was observed below 500 psfa free-stream static pressure for any of the configurations; however, the scale effects are such that burning could persist in the full-scale configuration to lower free-stream static pressures.

The effect of off-trajectory altitude on base heating at M_∞ = 1.2 is shown in Fig. 20. At trajectory altitude (29,000 ft) base heating was extensive; however, a small increase in altitude resulted only in localized heating. At 42,000 ft, the base heating from the turbine exhaust was essentially eliminated.

As shown in Fig. 21, the increase in heating due to the turbine exhaust was essentially the same at 0 deg and -4 deg angle of attack; however, the increase in heat flux around the top engine (number 2) at -7 1/2 deg angle of attack was the highest noted during the test.

Since the failure of one of the engines would not necessarily abort a flight, it was desirable to determine the effect of an inoperative engine on the base heating. This condition was investigated with the number 7 engine inoperative. The increase in heat flux decreased around the top (number 2) engine and increased near the side engine (number 3) as shown in Fig. 22. Small but negligible effects were noted for the turbine-exhaust-off heating rates.

BASE PRESSURES

The ratio of base pressure to free-stream static pressure for the primary heat shield is shown in Fig. 23 for trajectory conditions. Operation of the engines resulted in an increase in base pressure as would be expected. At $M_\infty = 1.2$ a significant increase in base pressure was observed when the simulated turbine exhaust was used. The effect was the same for all turbine exhaust configurations. The increase in base pressure was not influenced by the exhaust stack configuration and is believed to be attributable to the change in the jet wake caused by the exhausterators.

The ratio of base pressure on the star shield to free-stream static pressure is shown in Fig. 24. Comparison of the star shield base pressure ratios with the primary shield base pressure ratios (shown dashed) indicates high aspiration at the low Mach numbers, and the equalized pressures at $M_\infty = 1.4$ and 1.5 indicate the transition to backflow, as was also shown by the star shield heating (Fig. 15).

The effect of higher trajectory altitudes at $M_\infty = 1.2$ is shown in Fig. 25. The base pressure ratios for turbine-exhaust-off operation were found to be a linear function of the free-stream static pressure and increased as the free-stream static pressure was reduced. At the higher altitudes (lower pressures) the change in base pressure produced by the turbine exhaust was negligible. The effect of the engine exhaust on the base pressure was small at the higher pressures and very large at the lower pressures. The higher Mach number data at comparable free-stream static pressures indicate that the power on base pressure is also dependent upon Mach number as well as free-stream static pressure.

CONCLUSIONS

1. Simulated turbine exhaust flow caused increased star shield equilibrium wall temperatures and lower film coefficients for all exhaust stack configurations at the lower Mach number and altitude trajectory conditions.
2. Negligible effects of the turbine-exhaust on star shield heating at the maximum test Mach number indicated the transition from inner engine base aspiration to backflow occurred at this condition. Equalization of the primary heat shield and star shield pressures at these test conditions also showed this base flow transition.

3. Burning of the simulated turbine exhaust gases in the missile base did not occur when the streamline exhaust stacks were used. Burning did occur at some of the test conditions when the other exhaust stack configurations were used.

4. The base burning phenomenon was found to be influenced by trajectory altitude at $M_\infty = 1.2$ with near zero increases in heating rates due to the turbine exhaust at higher altitudes.

5. Increased base heating due to increasing the angle of attack was not significant below approximately 4 deg. At 7-1/2 deg, large increases in base heating were produced.

REFERENCES

1. Test Facilities Handbook, (5rd Edition). "Propulsion Wind Tunnel Facility, Vol. 3." Arnold Center, January 1961.

2. Delano, J. B. "Full-Scale Propulsion Testing in the 16-Foot Transonic Circuit, AEDC." AEDC-TN-58-31, June 1958.

3. Tempelmeyer, K. E., Windmueller, A. K., Estabrooks, B. B., and Pindzola, M. "Rocket Engine Testing Capabilities of the Propulsion Wind Tunnel Facility." AEDC-TN-58-17, April 1958.

TABLE 1

CALORIMETER DESCRIPTIONS AND CONSTANTS

Calorimeters and Thermocouples	Type	Calorimeter Constant $\rho\tau$	Slug Material	Remarks
T-1	Total	3.96	Copper	Slug cemented with insulating material
T-2 through T-10	Total	3.15		Slug cemented with insulating material
NT-3 through NT-10	Total	3.24		Glass rod supported slug
NR-3 through NR-7	Radiation	1.02		Glass rod supported slug behind a sapphire window
C-1 through C-2	Convection	2.32		Glass rod supported slug
A-2 through A-6	Gas Temperature			Platinum vs platinum + 10% rhodium

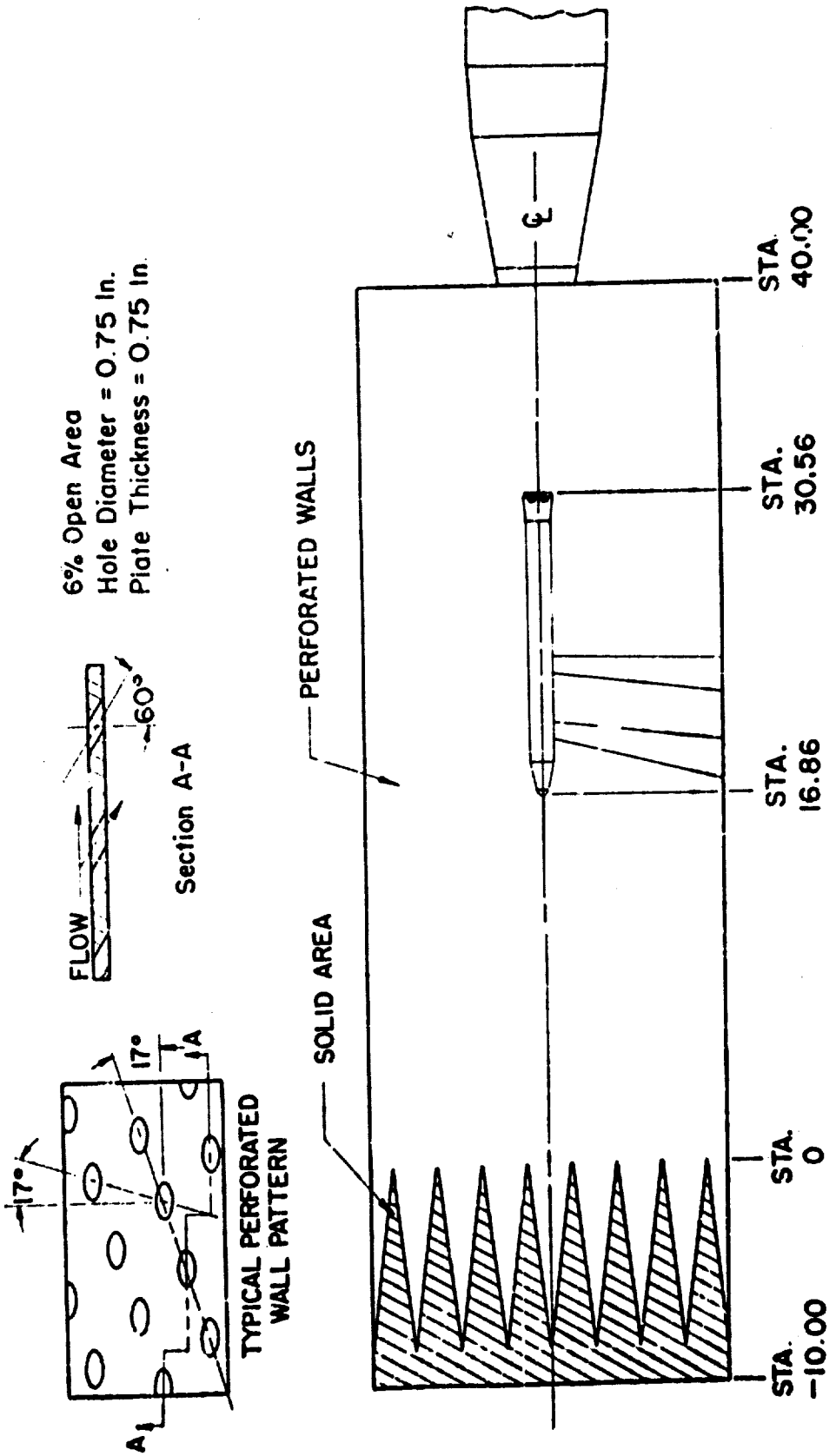

Fig. 1 Test Installation in Tunnel

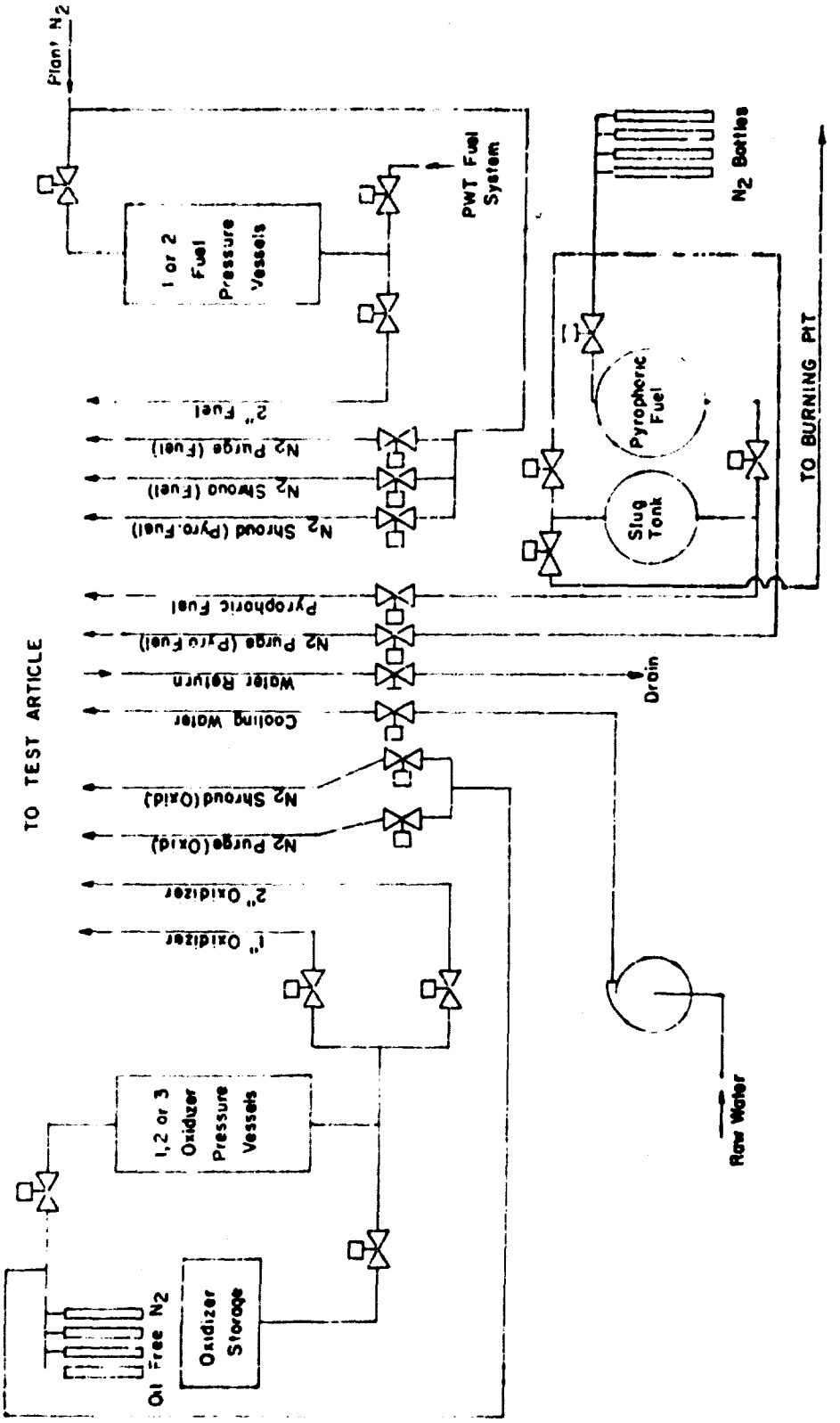

Fig. 2 Rocket Propellant System

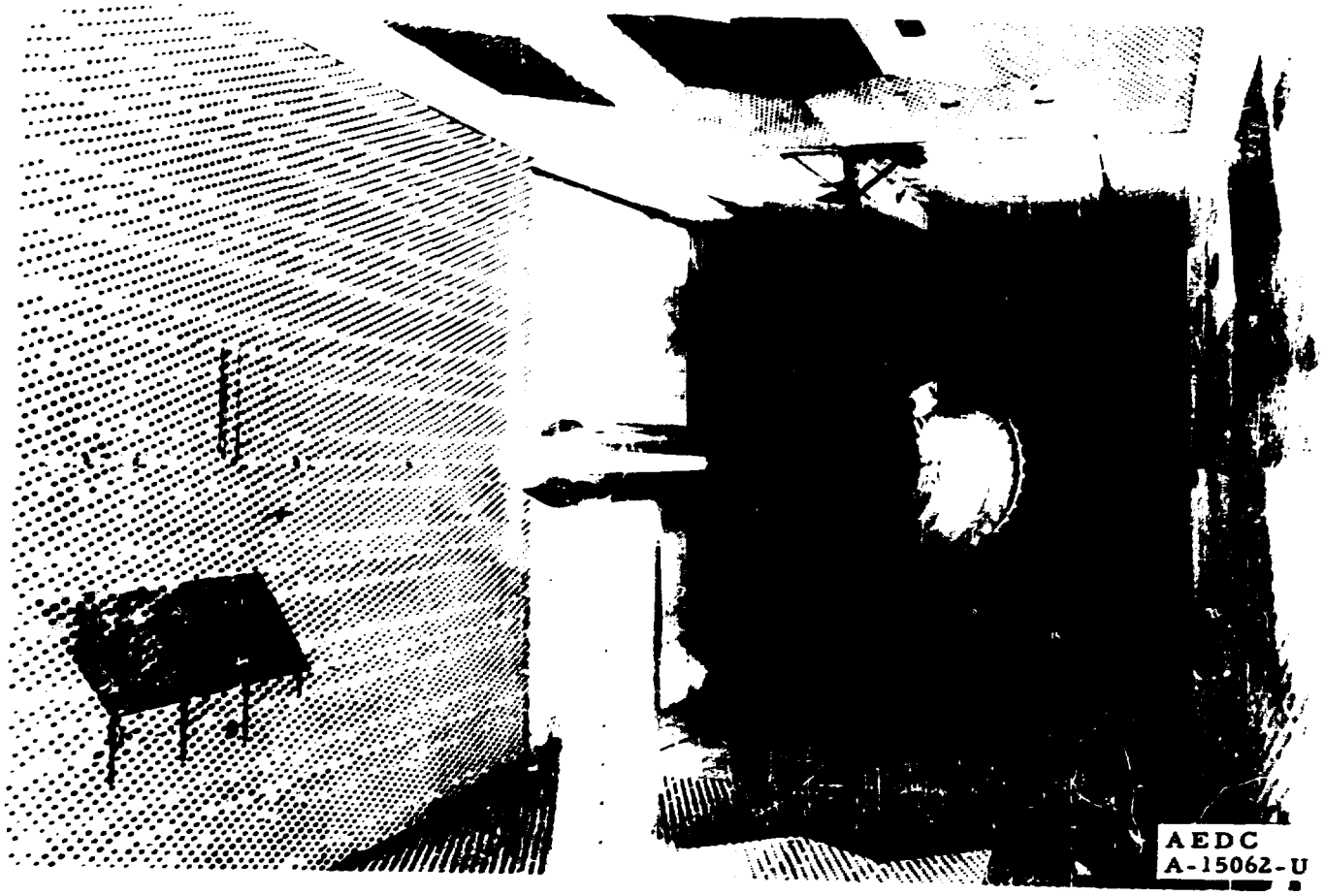

a. Front View

Fig. 3 Saturn Base Heating Model Tunnel Installation

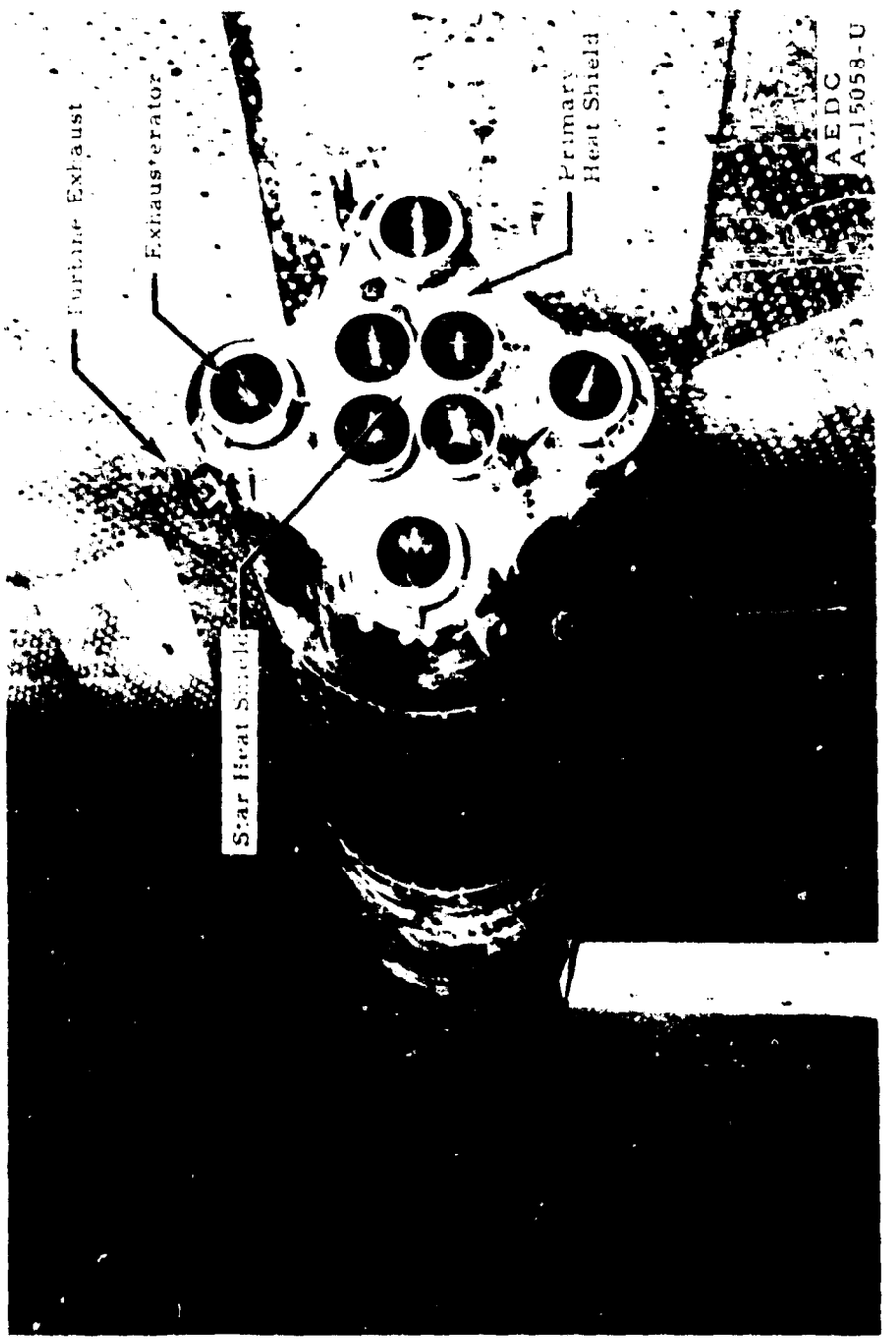

b. Rear View

Fig. 3 Concluded

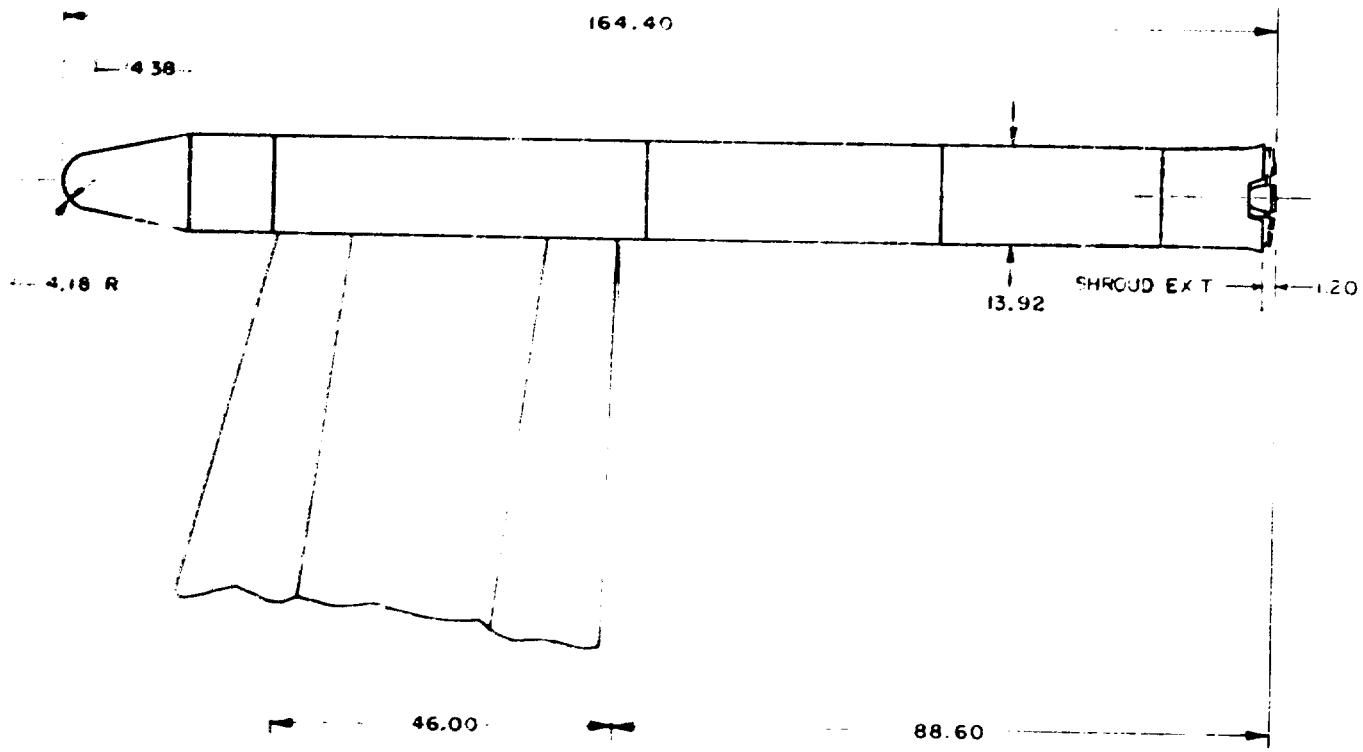

NOTE: ALL DIMENSIONS ARE IN INCHES

Fig. 4 Dimensional Sketch of Model Tested

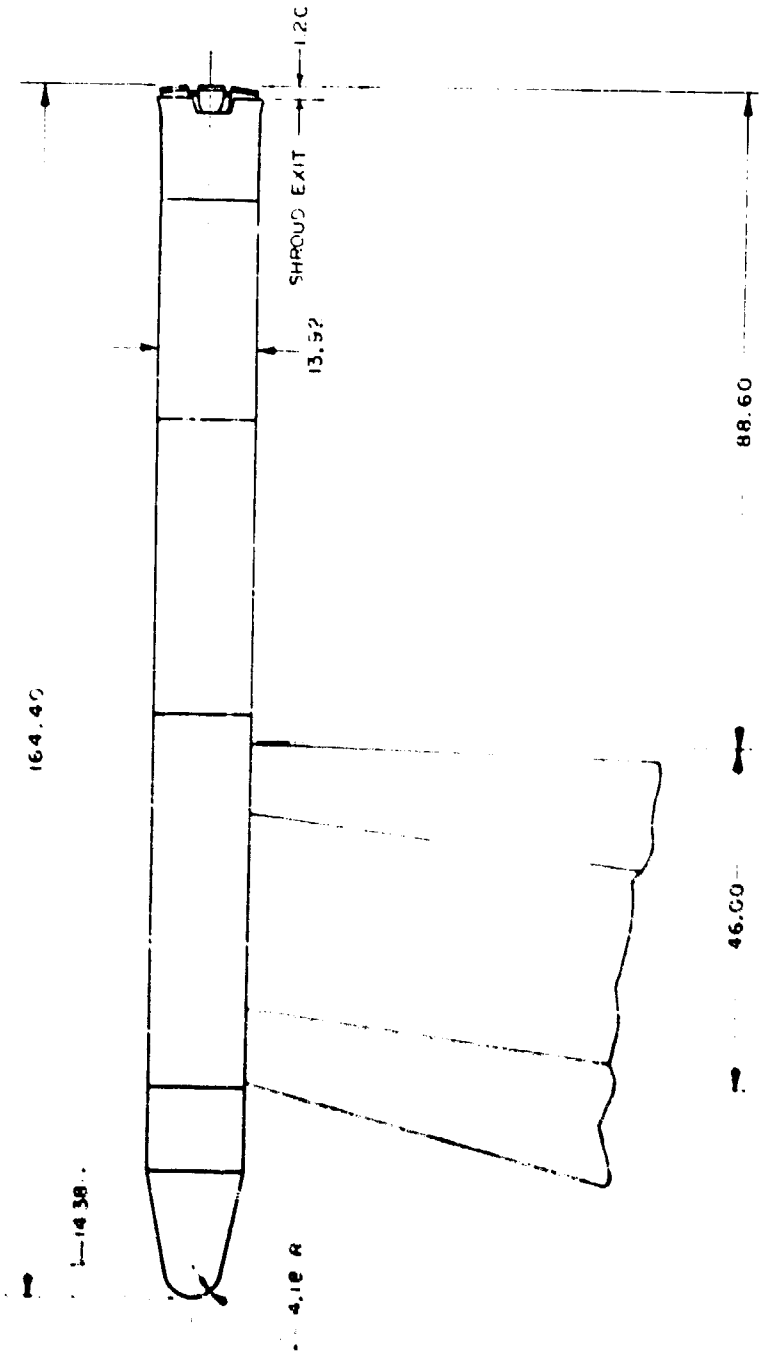

NOTE: ALL DIMENSIONS ARE IN INCHES

Fig. 4 Dimensional Sketch of Model Tested

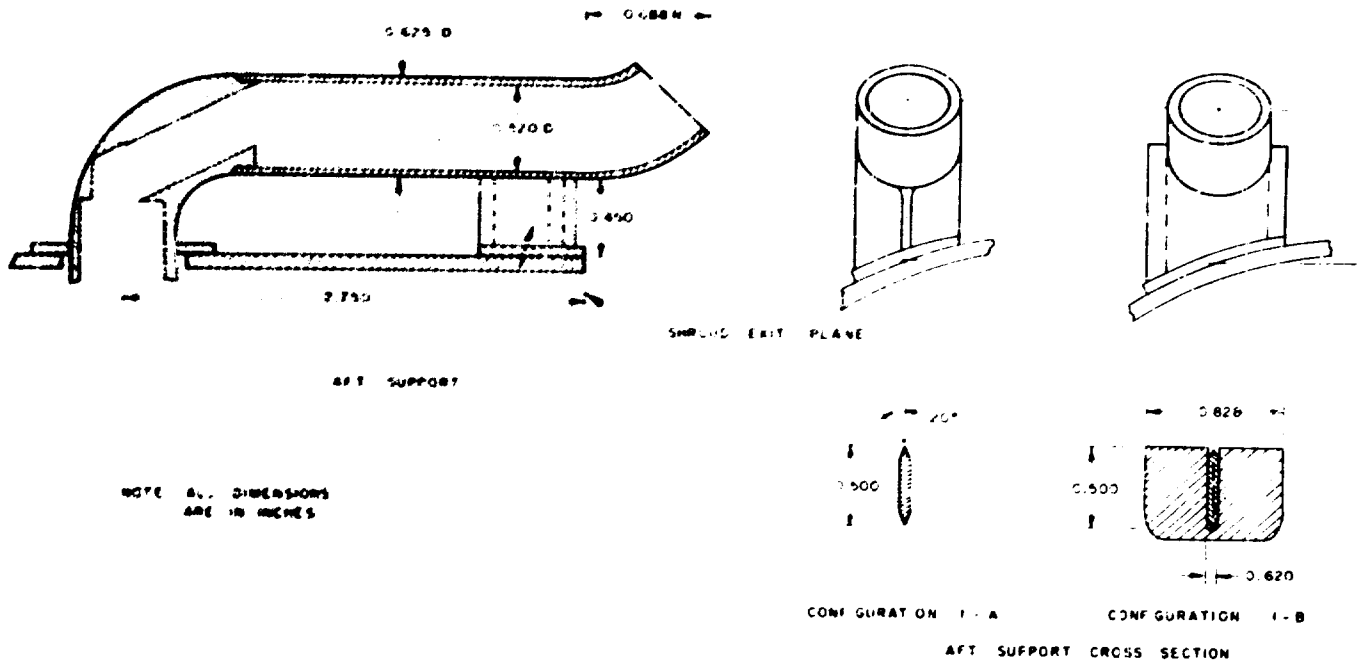

Fig. 5 Exhaust Stack Configuration 1-A and 1-B

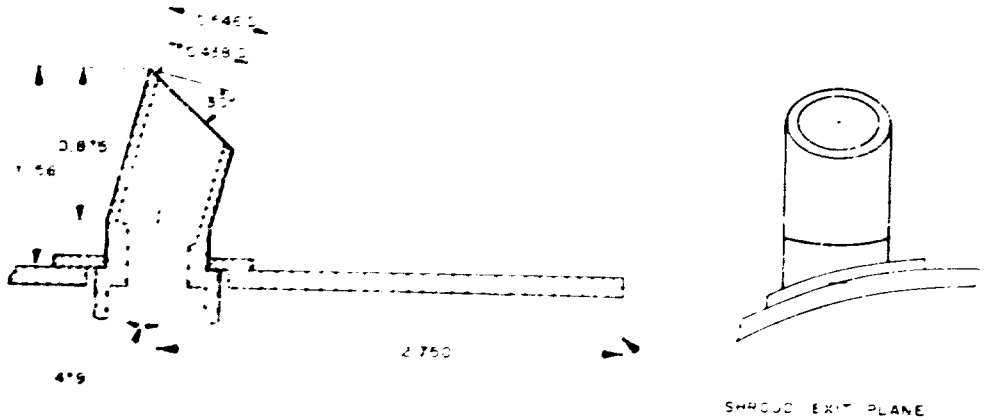

Fig. 6 Exhaust Stack Configuration 2

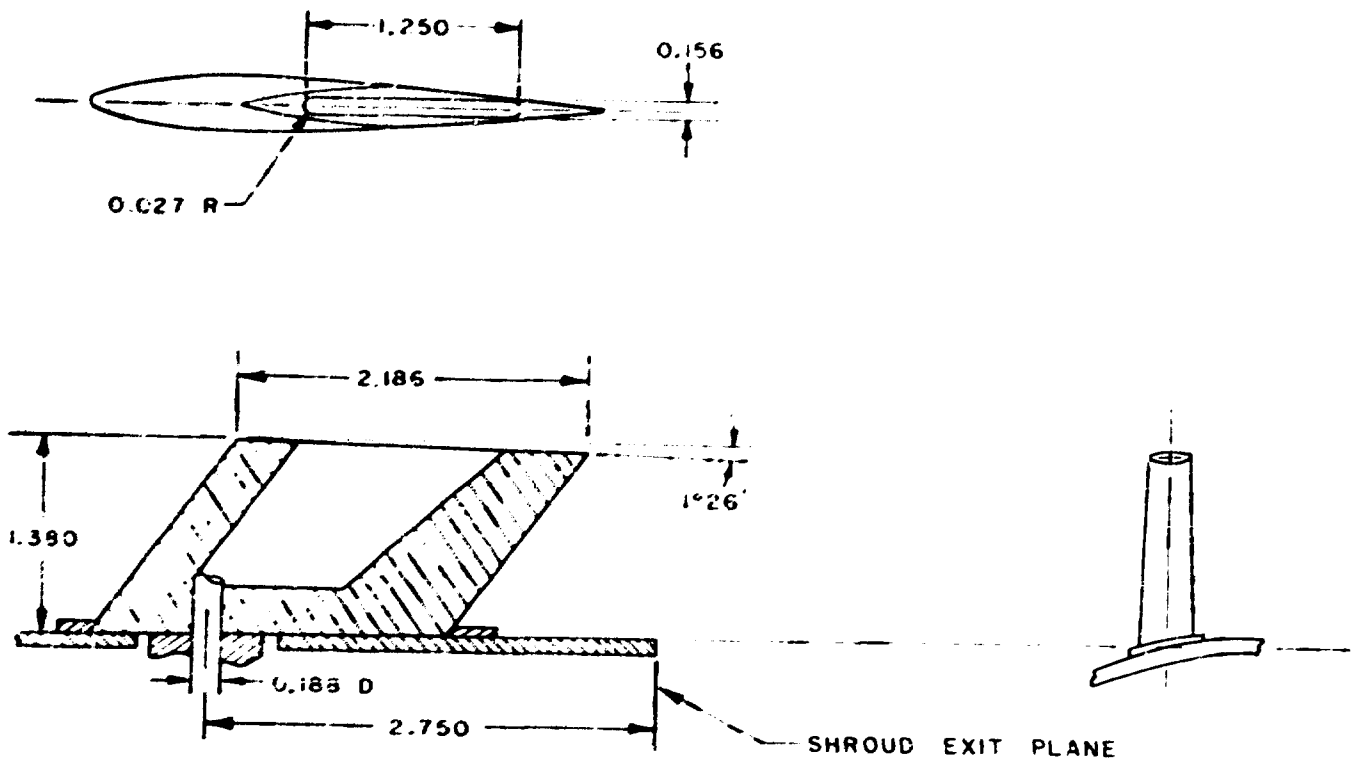

NOTE: ALL DIMENSIONS ARE IN INCHES.

Fig. 7 Exhaust Stack Configuration 3

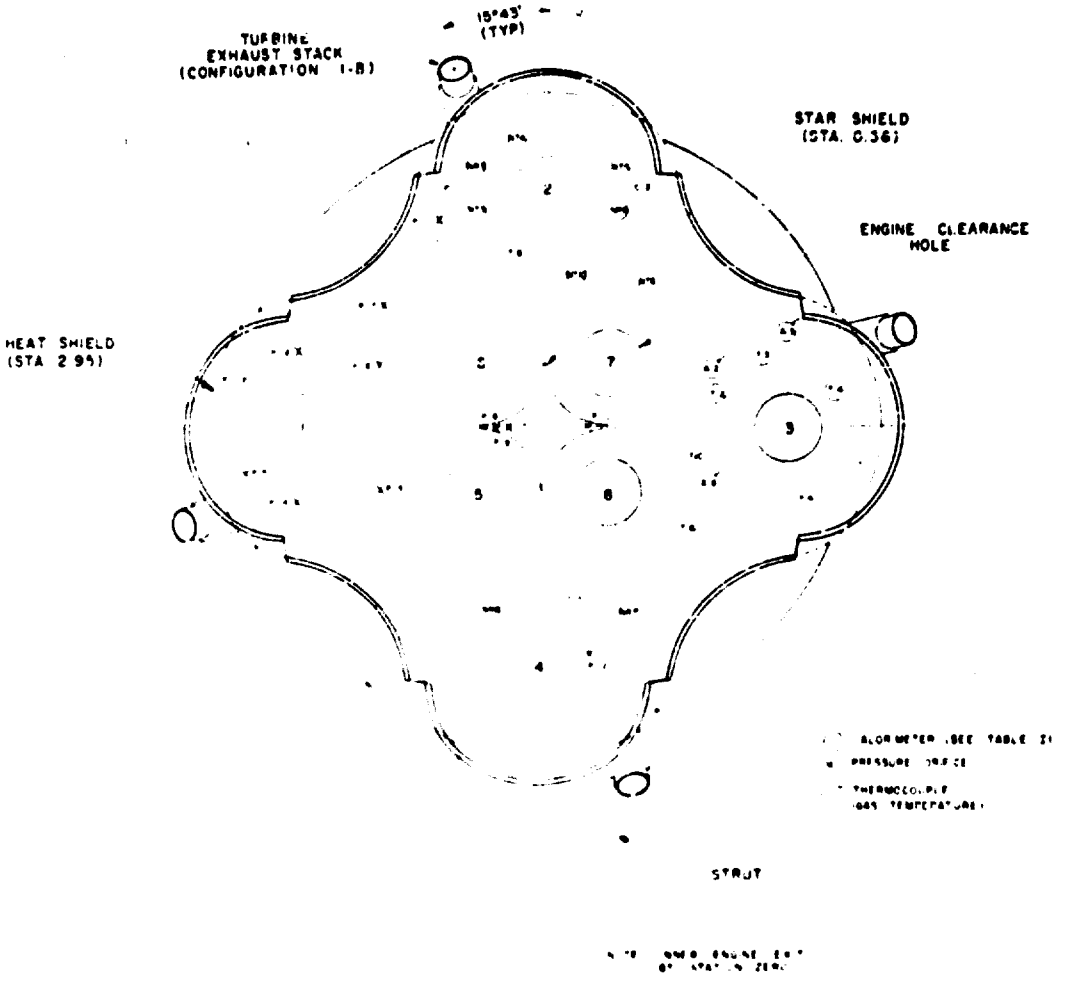

Fig. 8 Instrumentation Locations

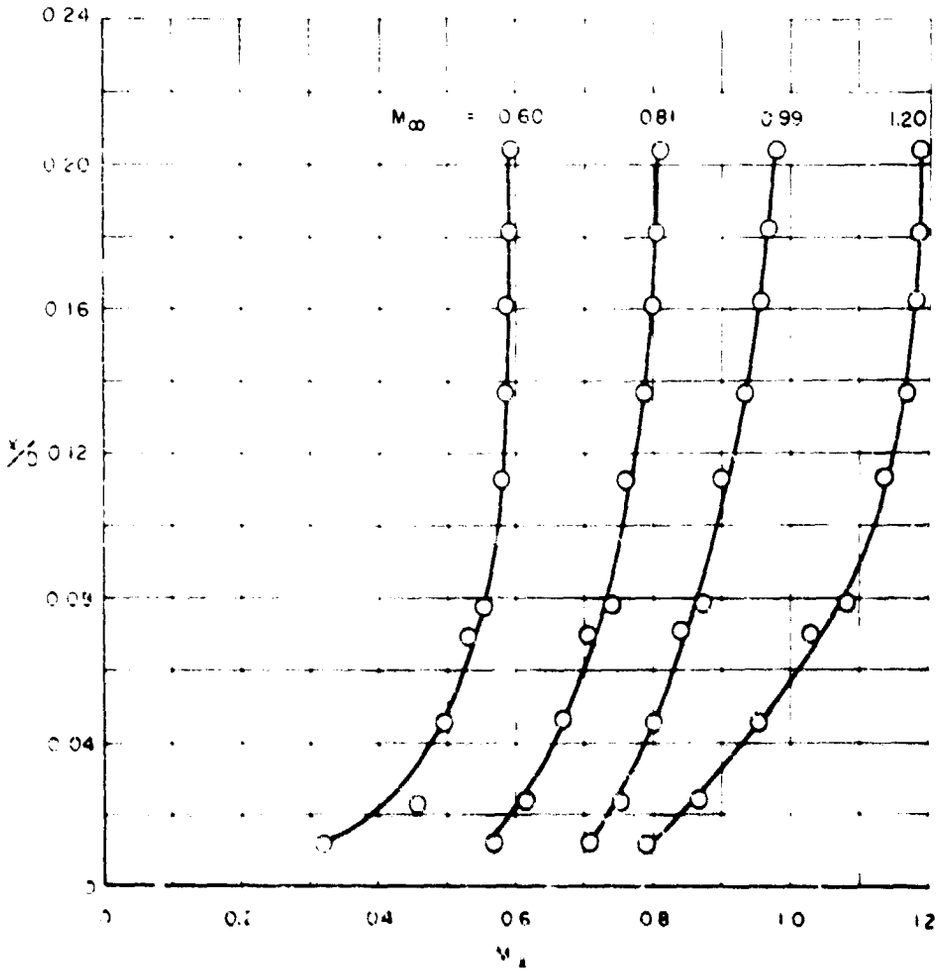

Fig. 9 Boundary-Layer Mach Number Distribution for Various Free-Stream Mach Numbers, $\alpha = 0$

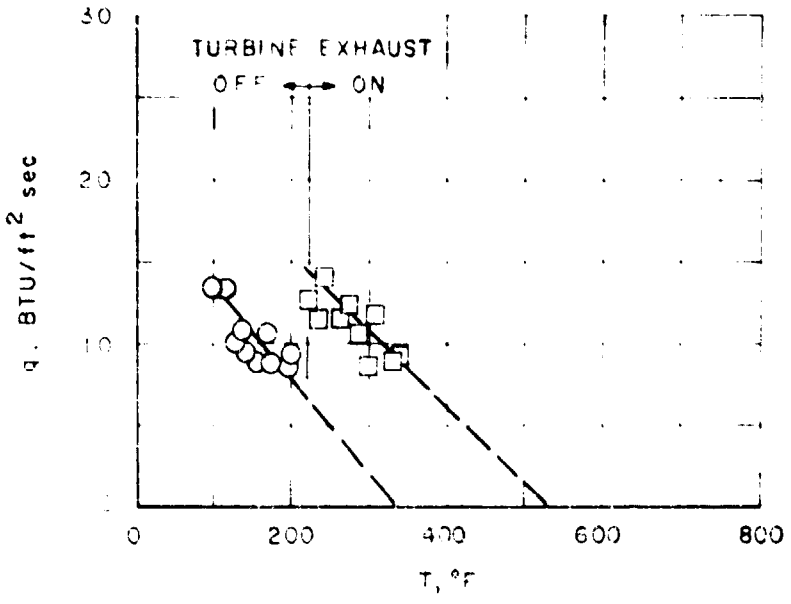

a. M_∞ - 0.6, Altitude 10,000 ft

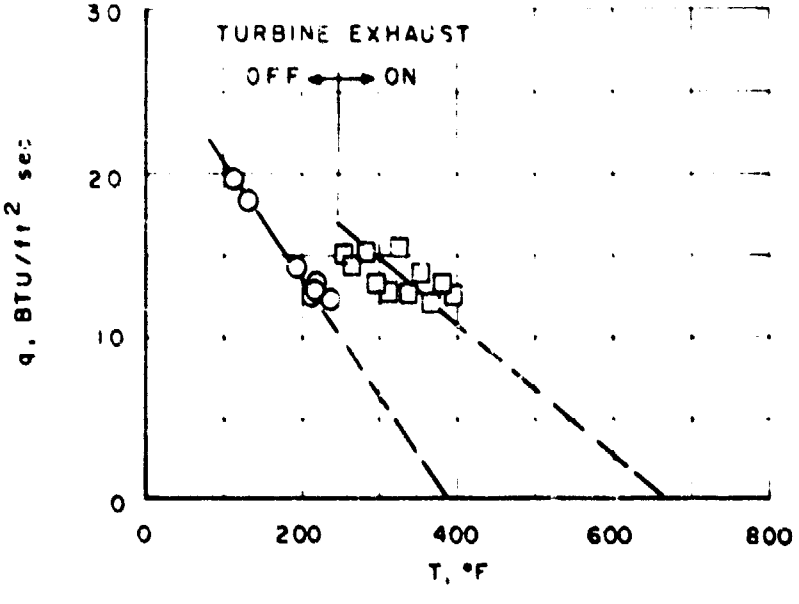

b. M_∞ - 0.8, Altitude 16,000 ft

Fig. 10 Star Shield Heating Rates as a Function of Calorimeter Temperature for Configuration 1-A

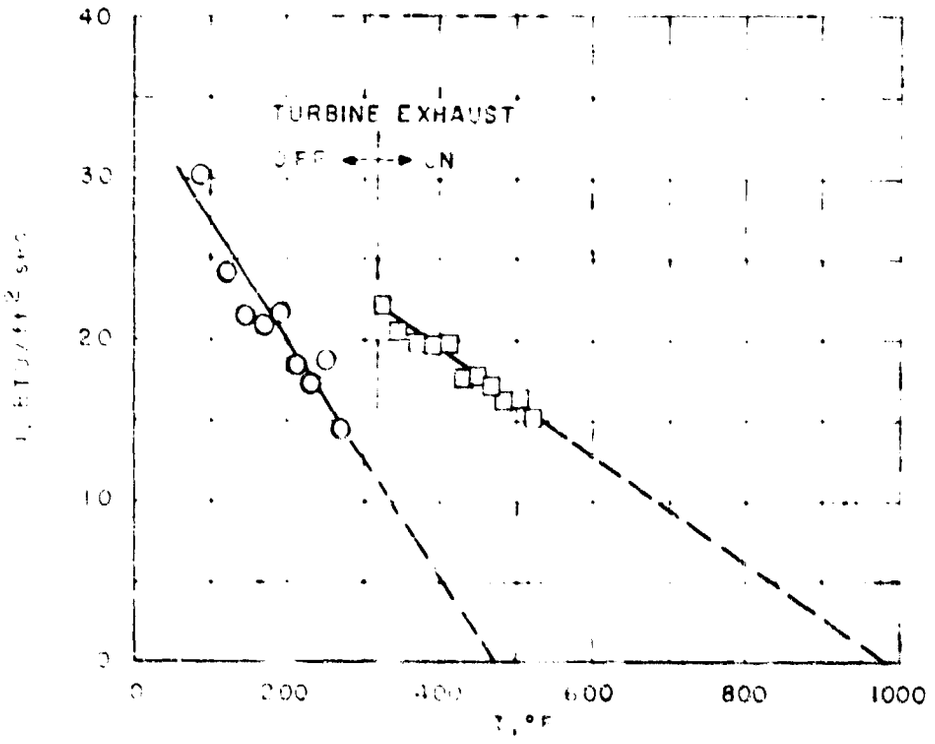

c. M_∞ 1.0, Altitude 22,000 ft

Fig. 10 Continued

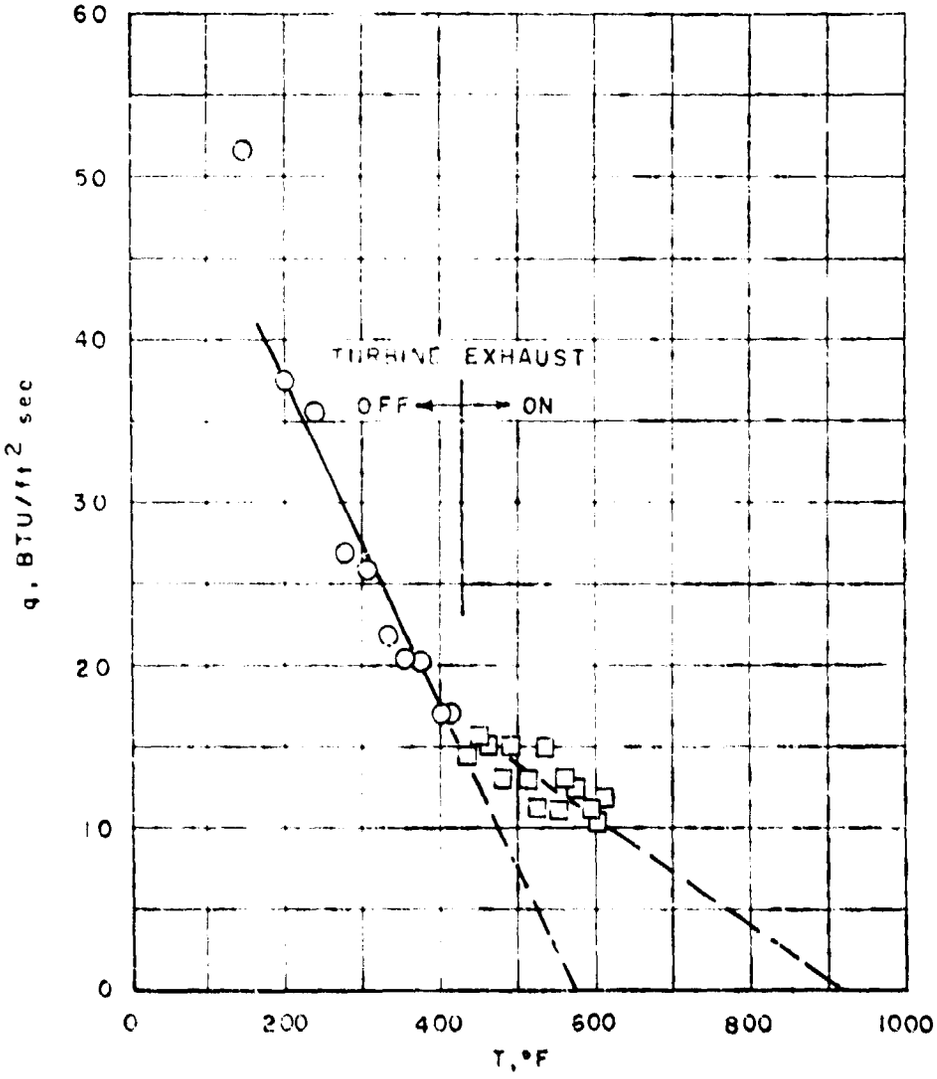

d. M_∞ = 1.2, Altitude 29,000 ft

Fig. 10 Continued

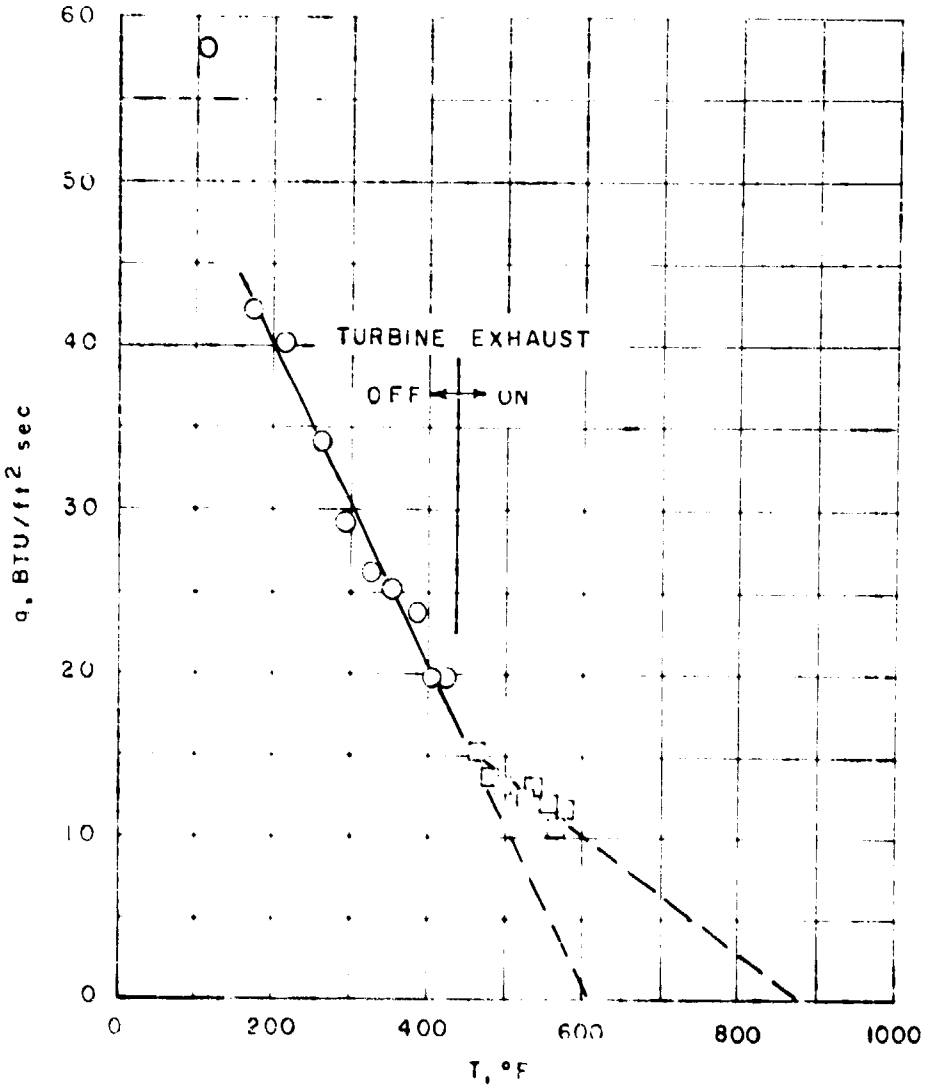

M, 1.2, Altitude 35,000 ft

Fig. 10 Continued

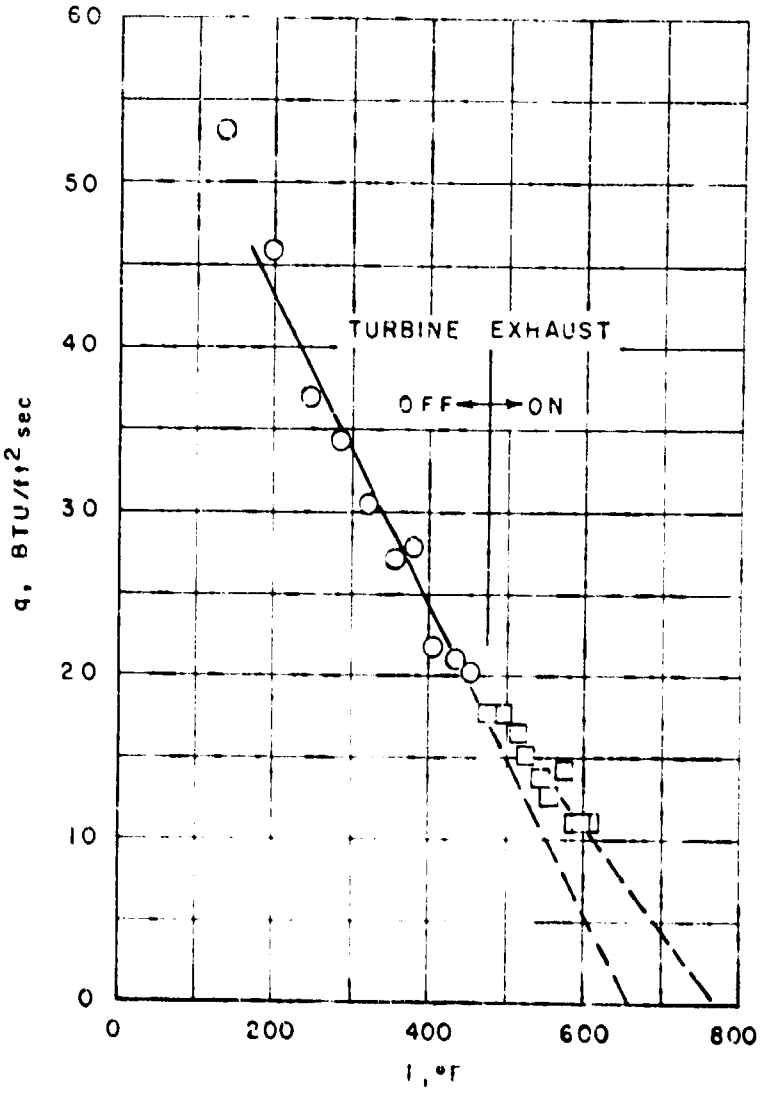

f. M_∞ = 1.2, Altitude 42,000 ft

Fig. 10 Continued

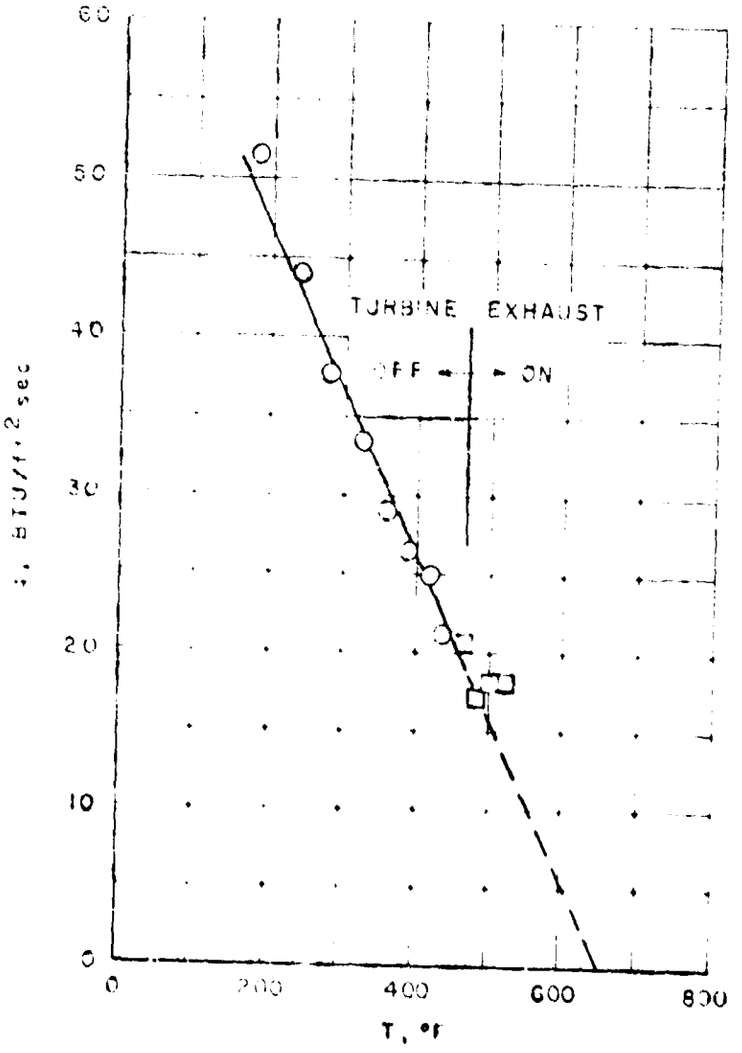

g. M_∞ = 1.4, Altitude 35,000 ft

Fig. 10 Continued

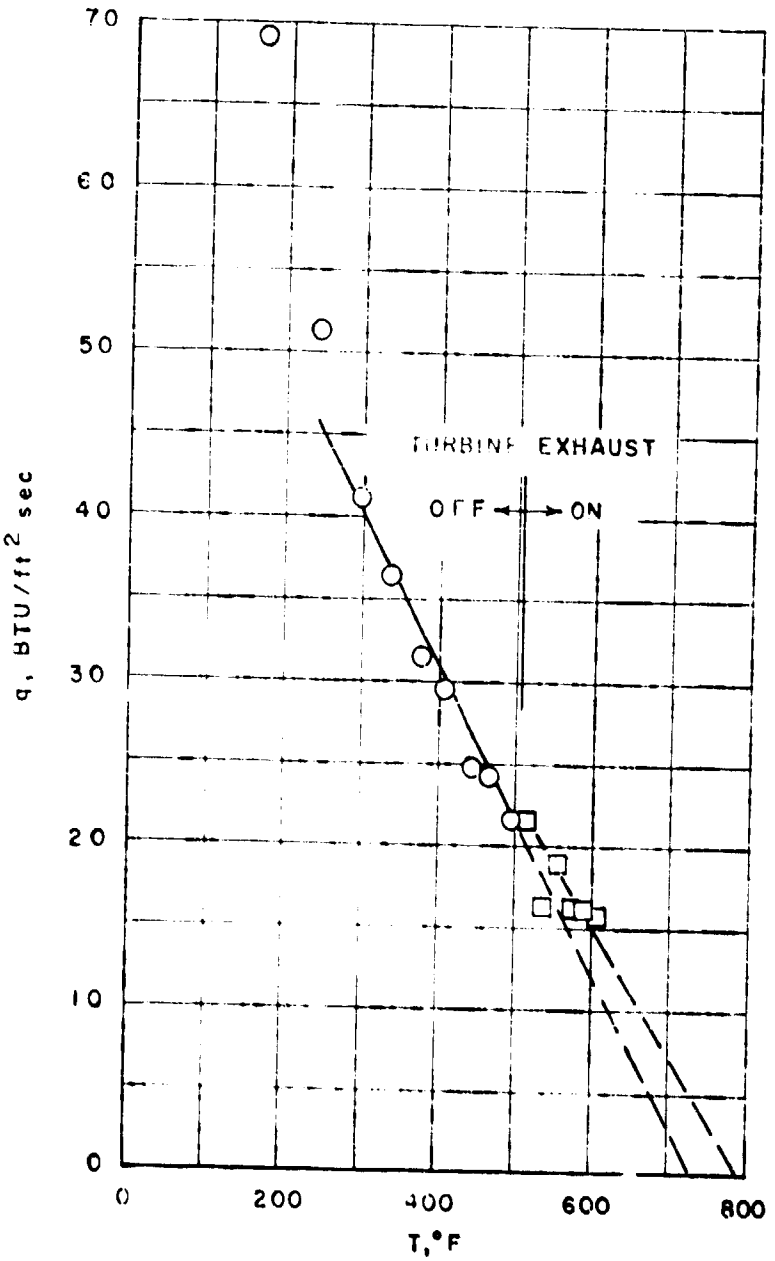

h. M_∞ = 1.5, Altitude 39,000 ft

Fig. 10 Concluded

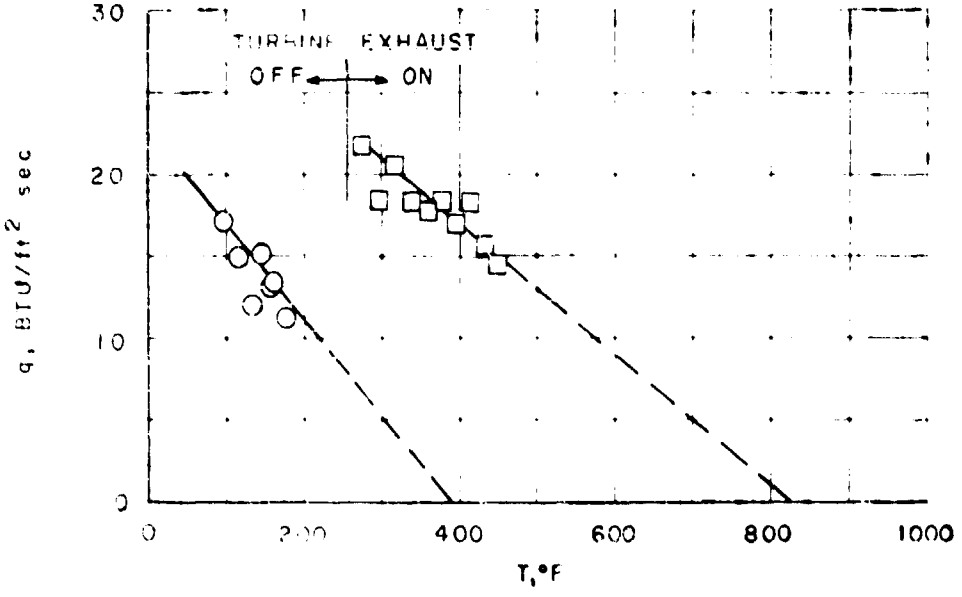

Fig. 11 Star Shield Heating Rates as a Function of Calorimeter Temperature, $M_\infty = 0.8$, Altitude 16,000 ft, Configuration 1-B

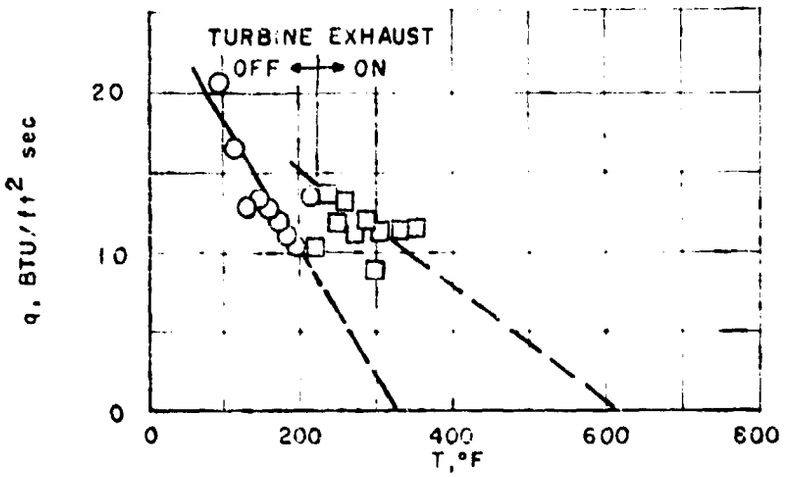

a. M_∞ = 0.8, Altitude 16,000 ft

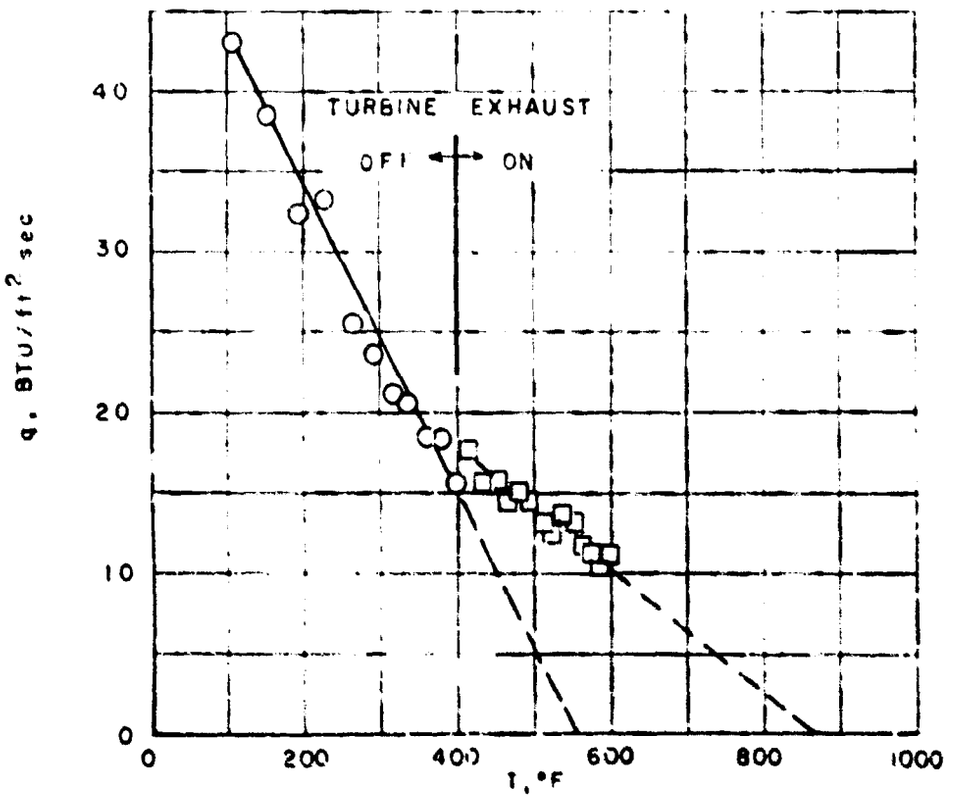

b. M_∞ = 1.2, Altitude 29,000 ft

Fig. 12 Star Shield Heating Rates as a Function of Calorimeter Temperature for Configuration 2

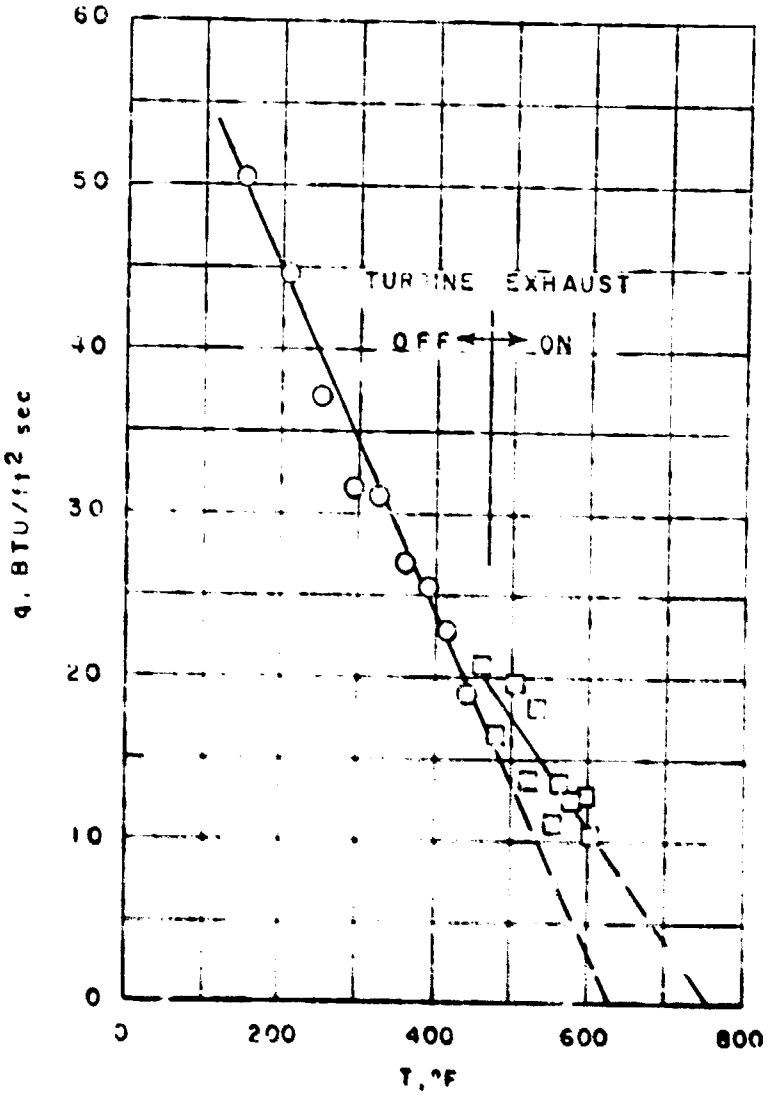

c. M_∞ = 1.5, Altitude 39,000 ft

Fig. 12 Concluded

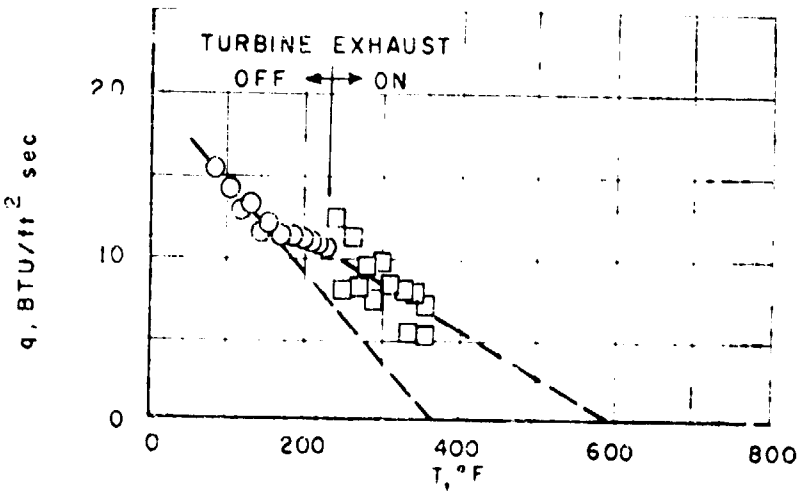

a. M_∞ = 0.8, Altitude 16,000 ft

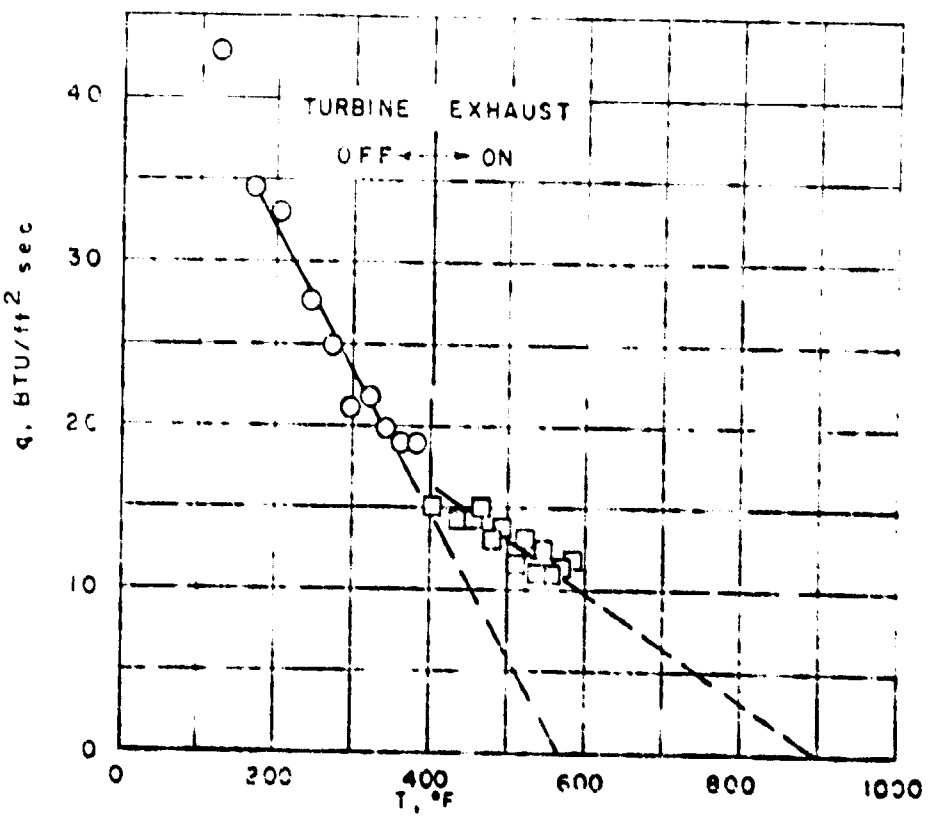

b. M_∞ = 1.2, Altitude 29,000 ft

Fig. 13 Star Shield Heating Rates as a Function of Calorimeter Temperature for Configuration 3

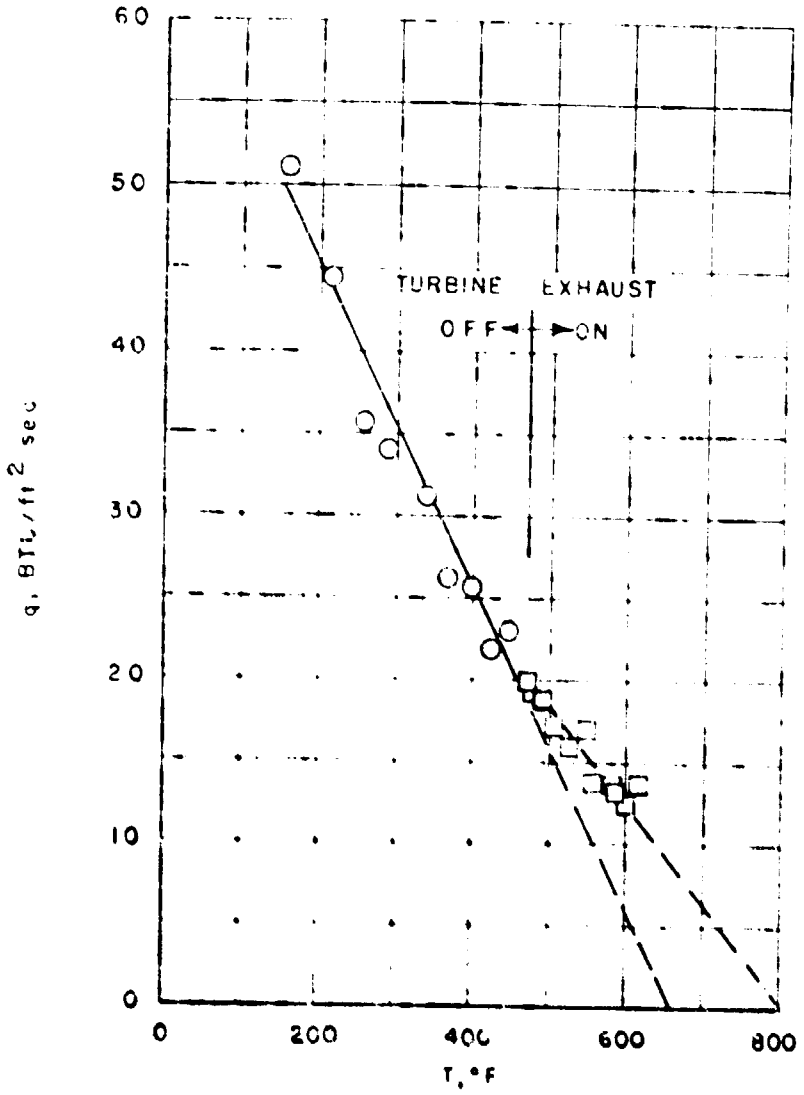

c. M_∞ = 1.5, Altitude 37,000 ft

Fig 13 Concluded

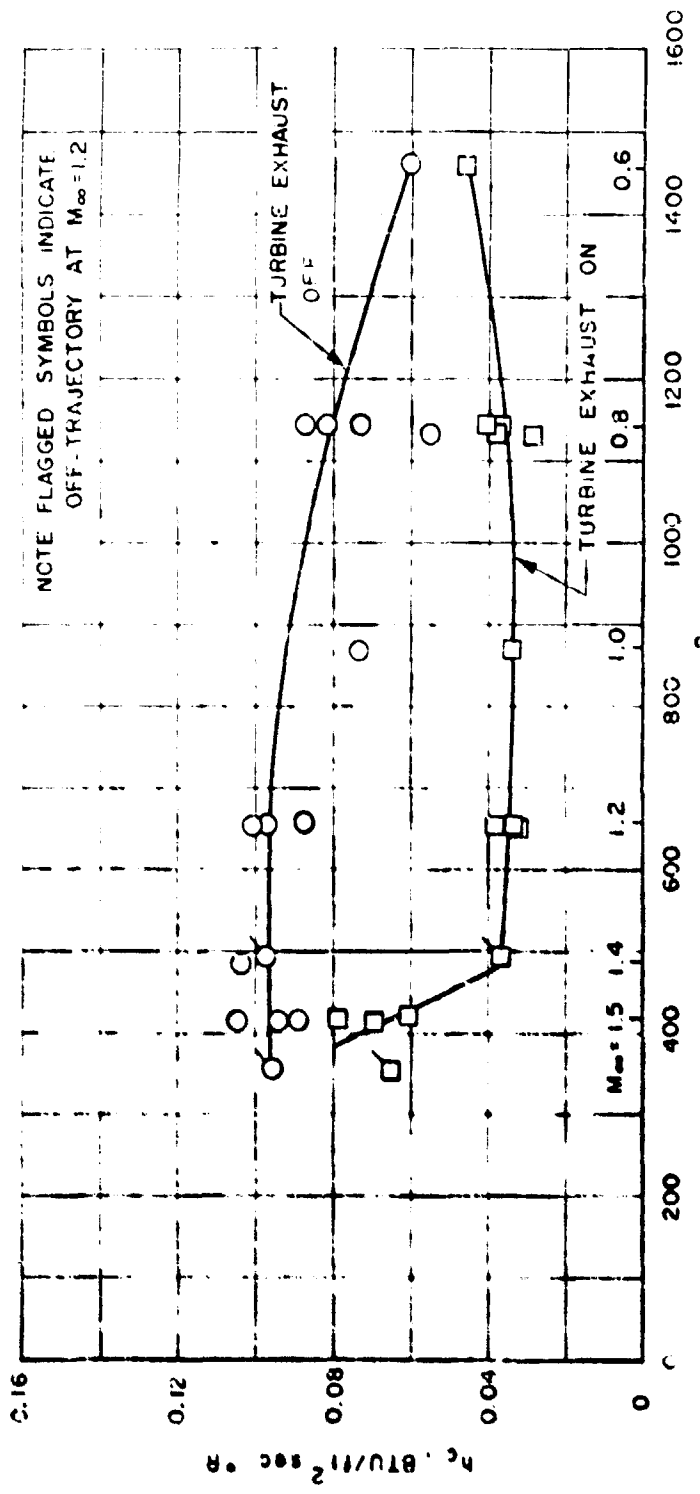

Fig. 14 Star Shield Experimental Film Coefficient

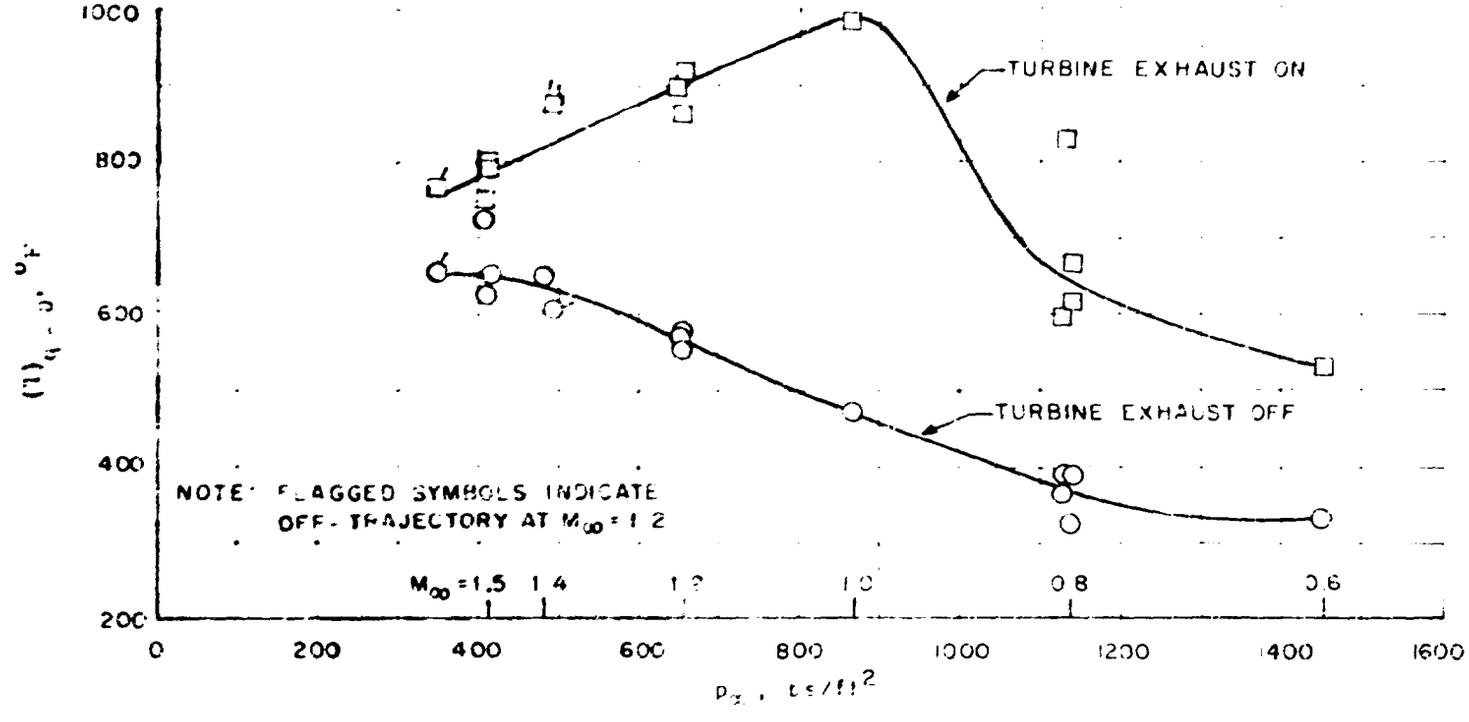

Fig. 15 Star Shield Equilibrium Temperature

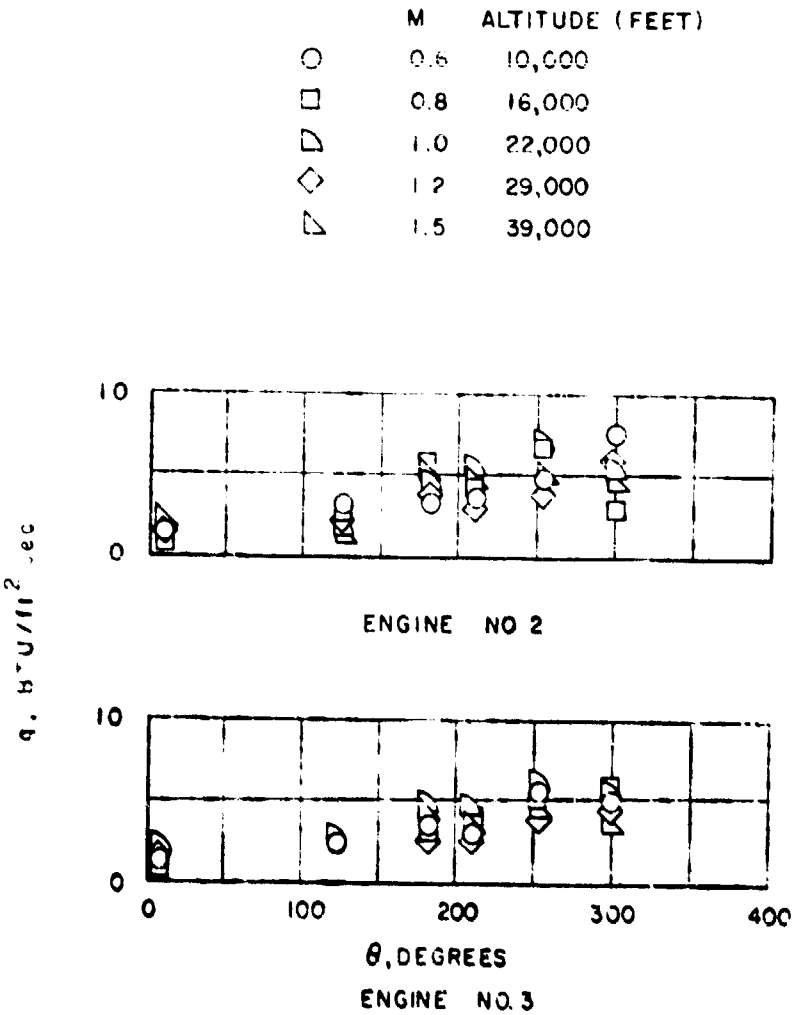

Fig. 16 Turbine Exhaust-Off Base Heating Rates for Various Calorimeter Locations with Trajectory Conditions as a Parameter

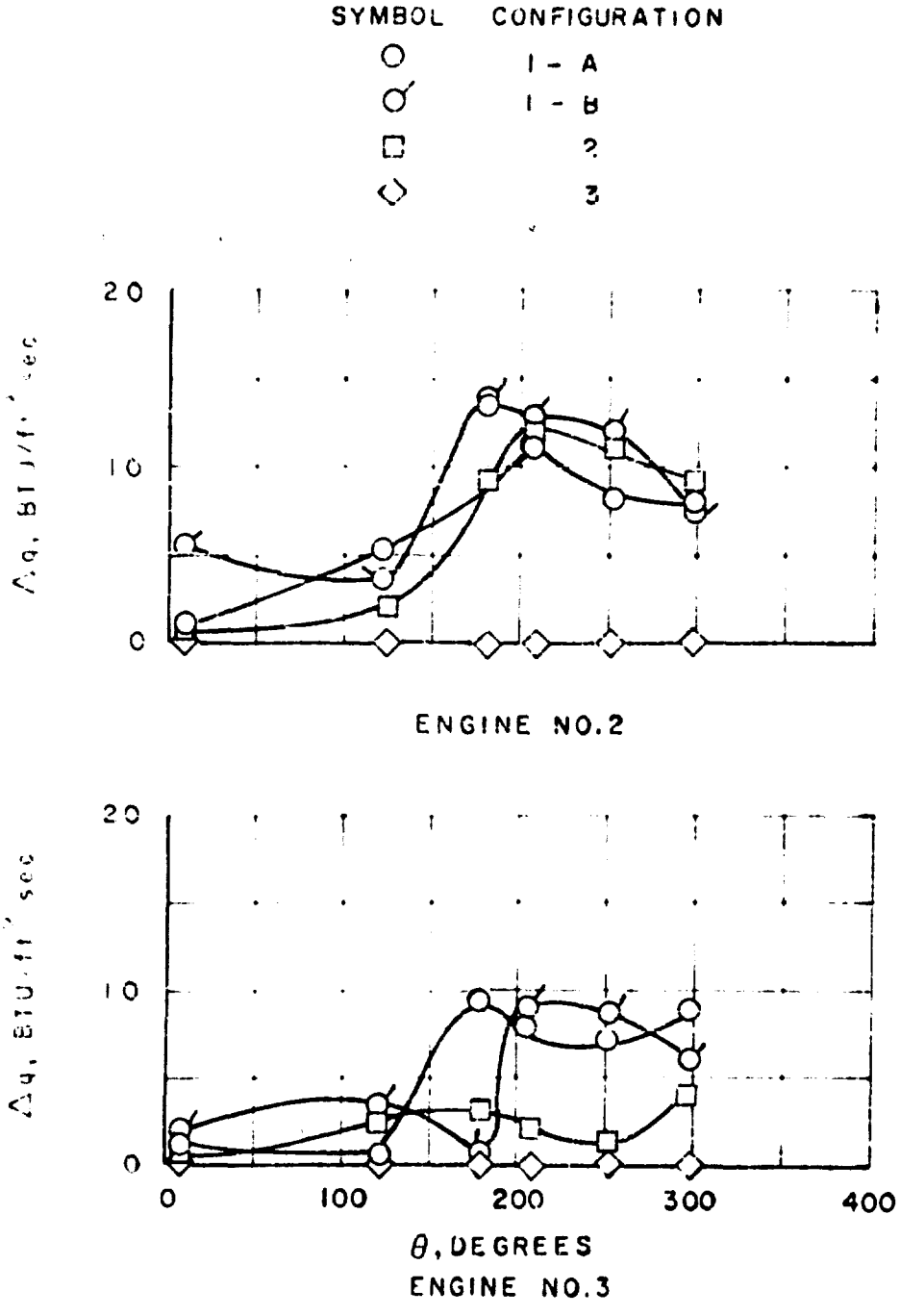

Fig. 17 The Increase in Base Heating Produced by Turbine Exhaust Operation for Various Exhaust Configurations, M_∞ = 0.8, Altitude 16,000 ft

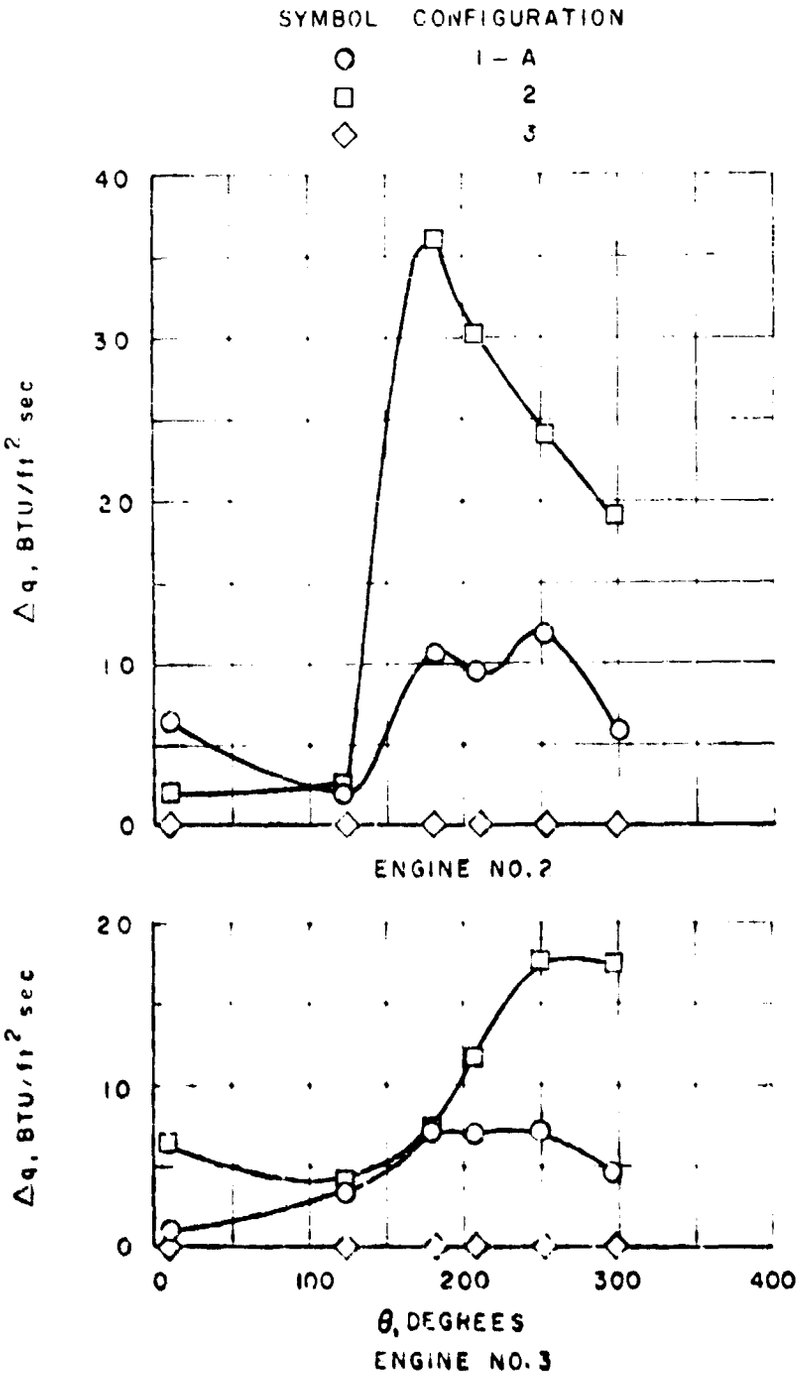

Fig. 18 The Increase in Base Heating Produced by Turbine Exhaust Operation for Various Exhaust Configurations, M_∞ = 1.2, Altitude 29,000 ft

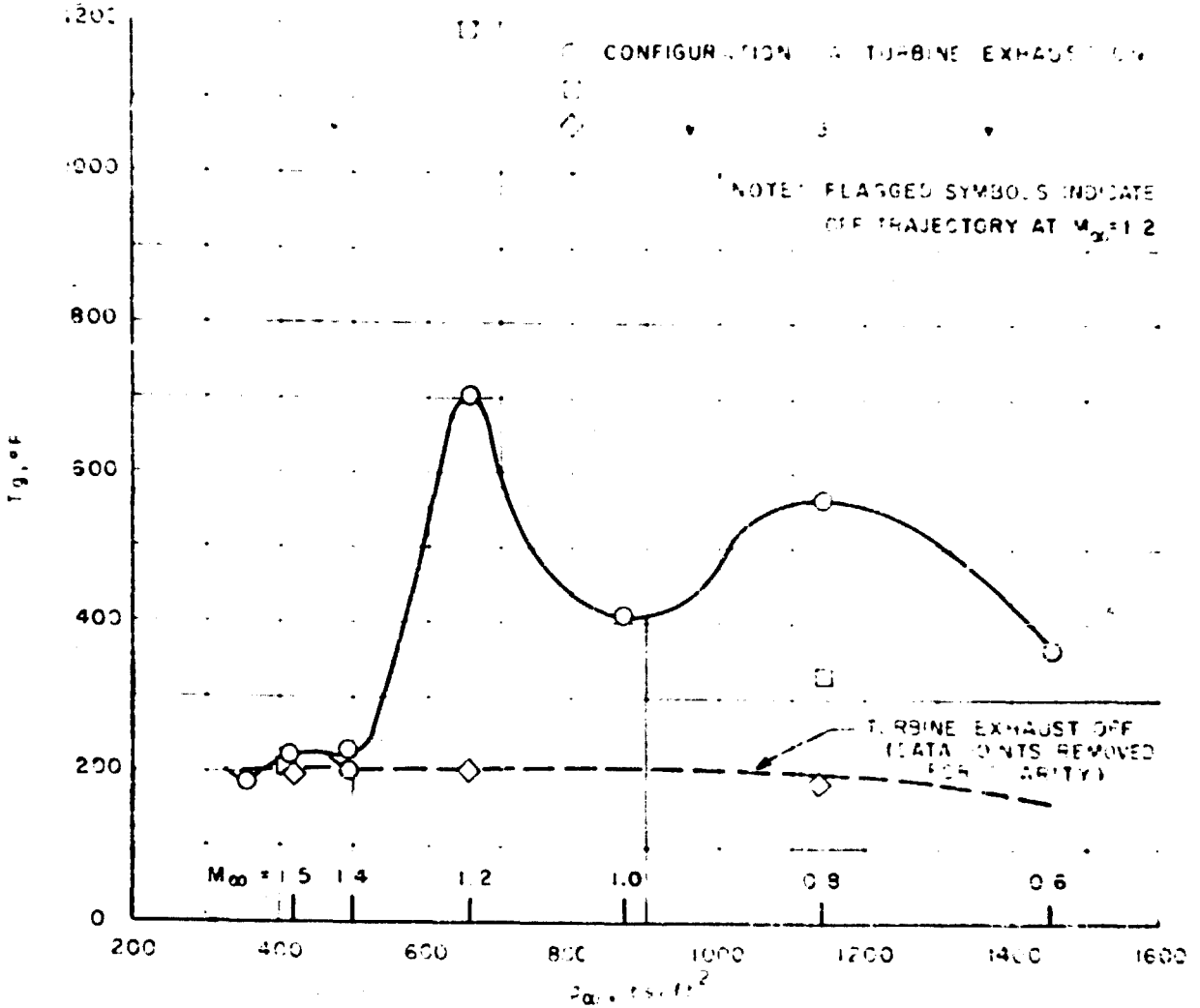

Fig. 19 Gas Temperatures Close to Primary Heat Shield for Trajectory Conditions

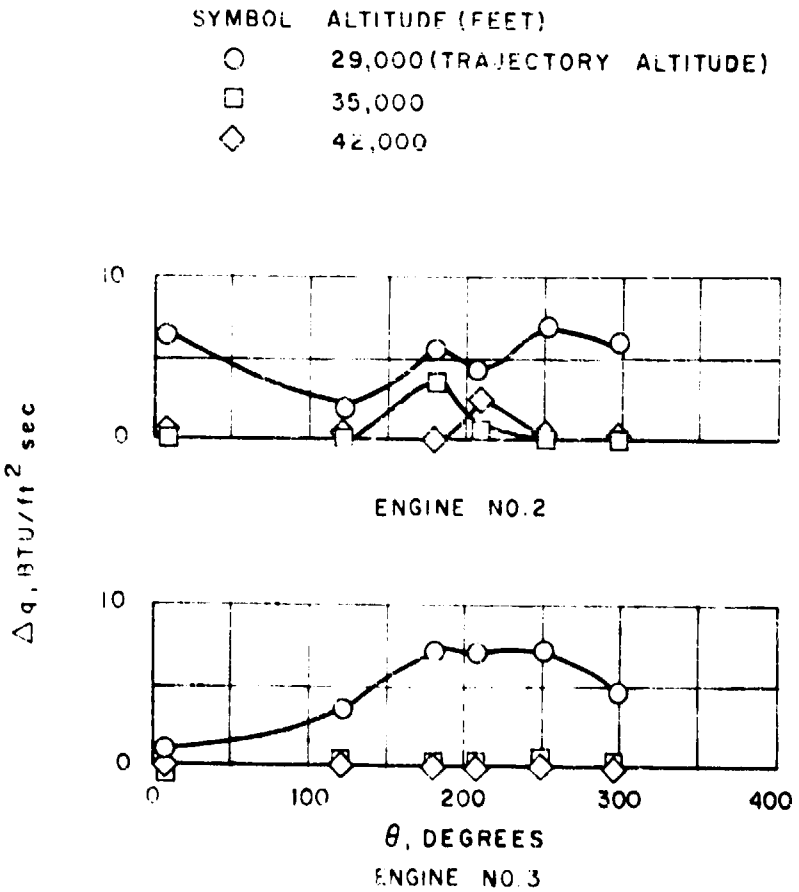

Fig. 20 The Increase in Base Heating Produced by Turbine Exhaust Operation for Various Altitudes, M_∞ = 1.2, Configuration 1-A

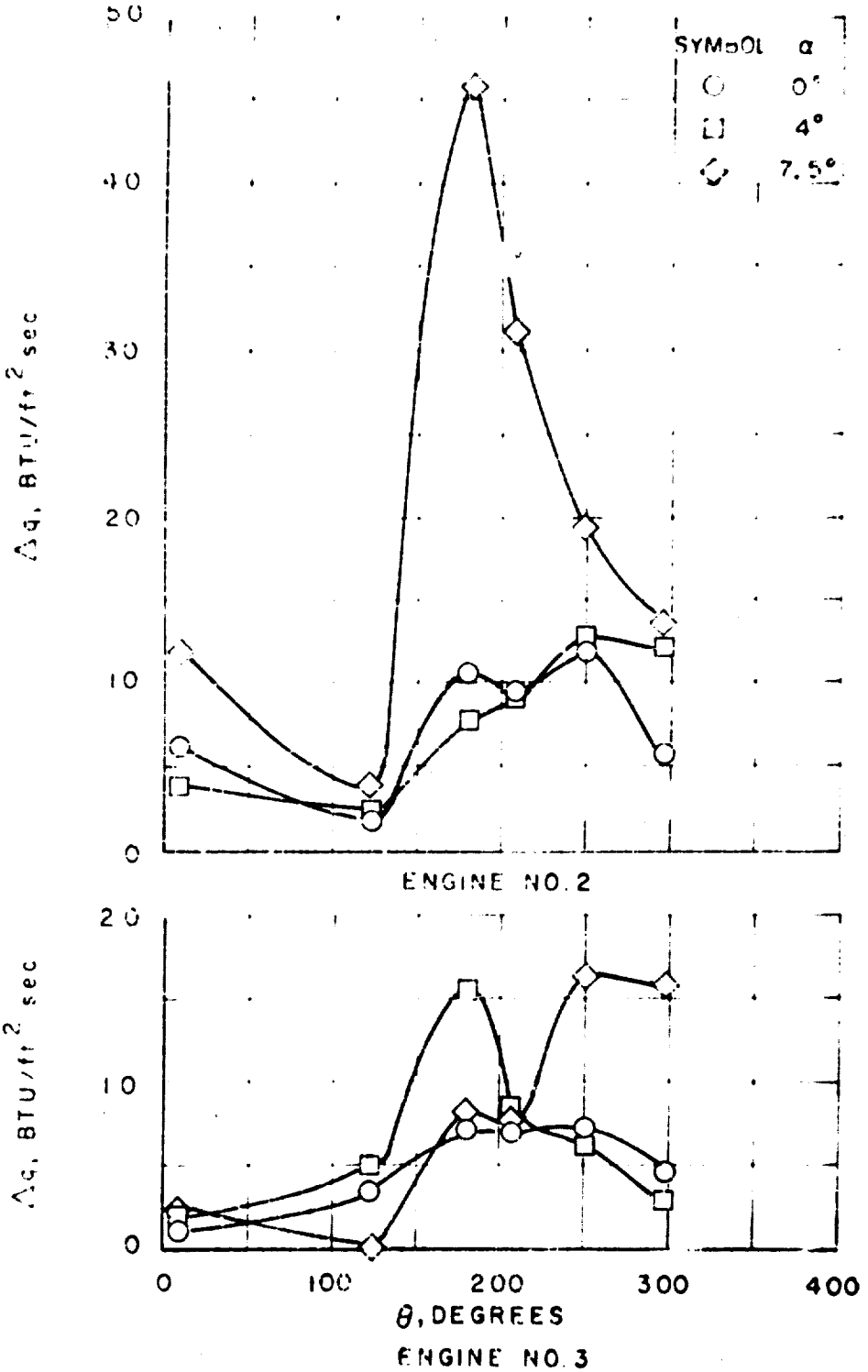

Fig. 21 The Increase in Base Heating Produced by Turbine Exhaust Operation for Various Angles of Attack, M_∞ = 1.7, Altitude 29,000 ft, Configuration 1-A

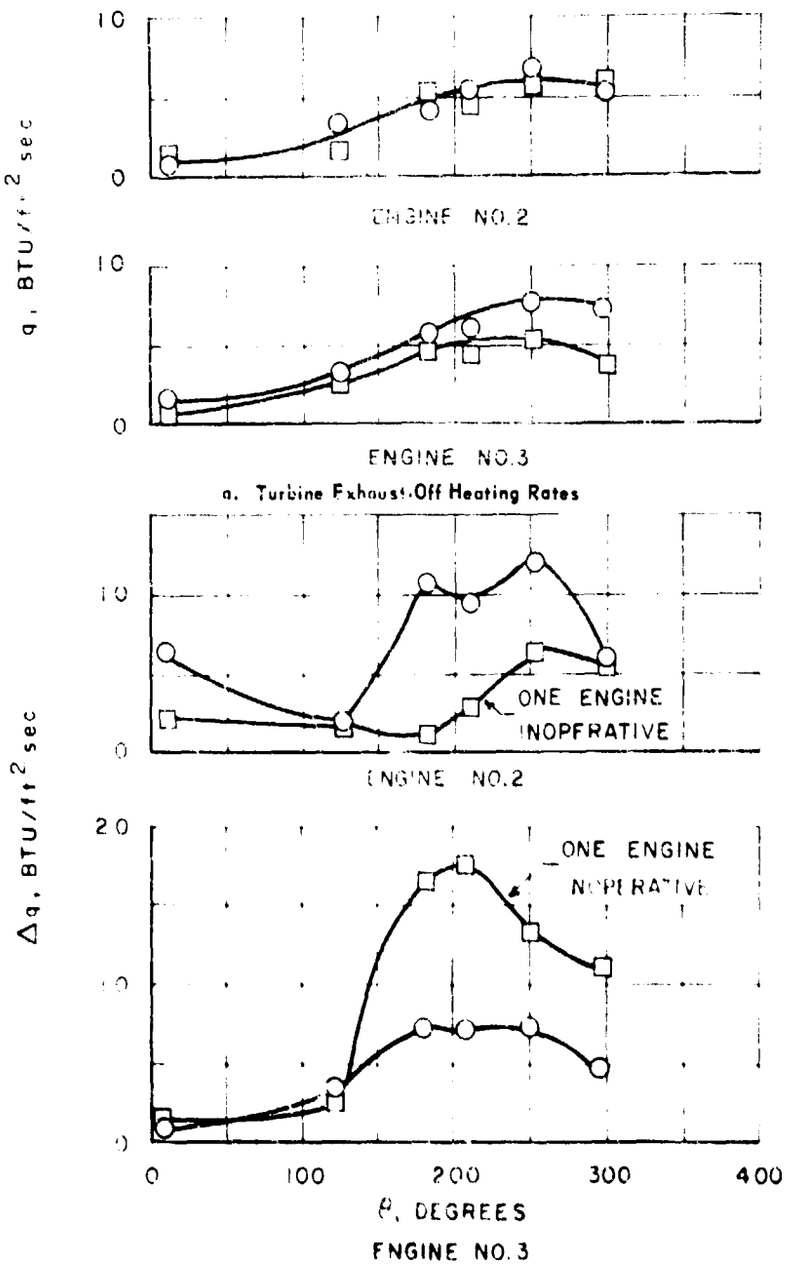

a. Turbine Exhaust-Off Heating Rates

b. Increase Produced by Turbine Exhaust Operation

Fig. 22 Comparison of One-Engine-Inoperative and Normal-Operation Base Heating Rates, $M_\infty = 1.2$, Altitude 29,000 ft, Configuration 1 A

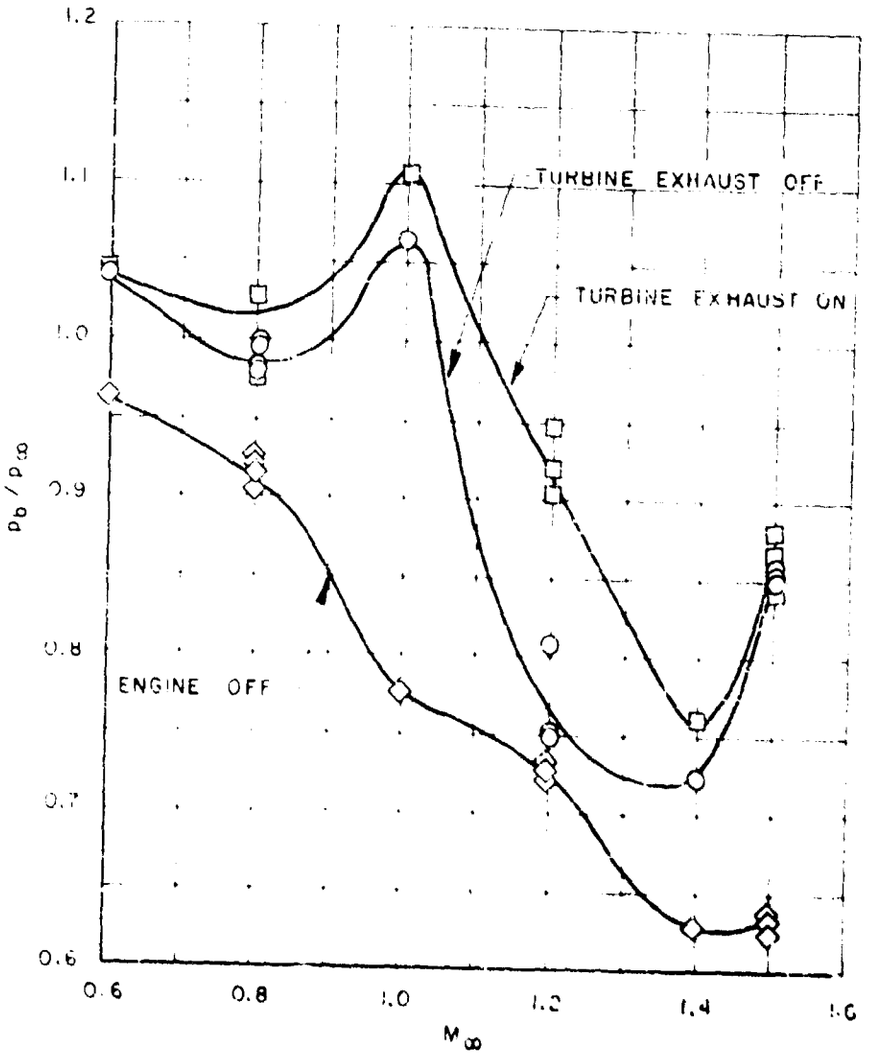

Fig. 23 Base Pressure Ratio for Trajectory Conditions on the Primary Heat Shield

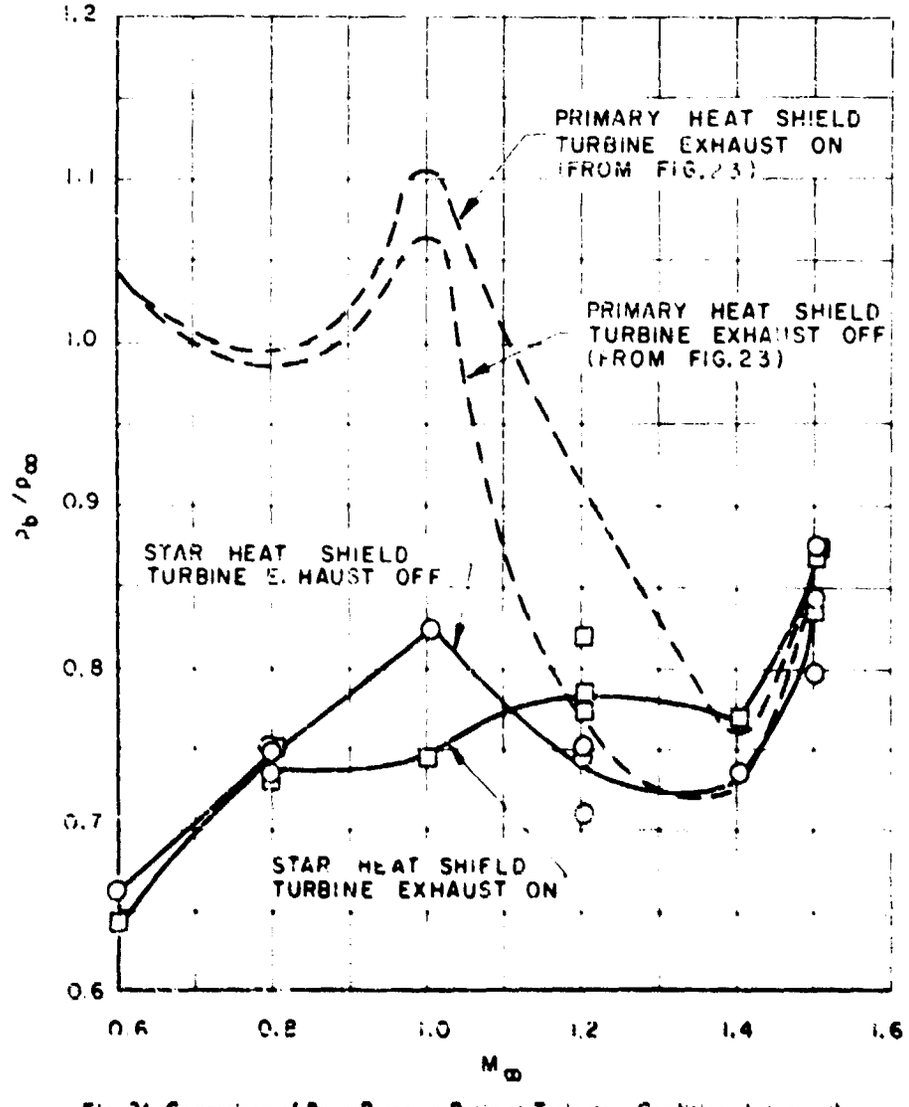

Fig. 24 Comparison of Base Pressure Ratio at Trajectory Conditions between the Primary and Star Heat Shields

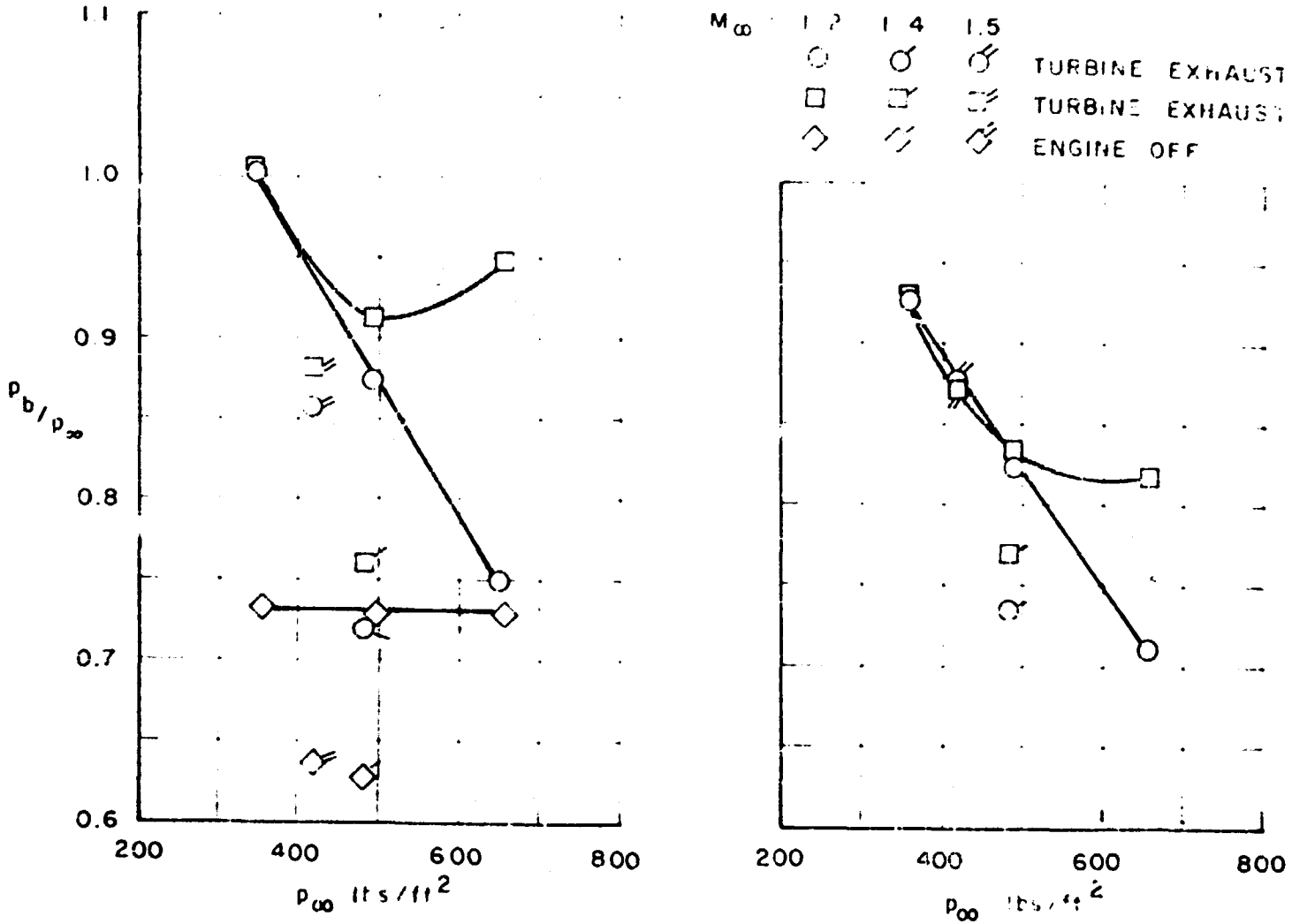

a. Primary Heat Shield

b. Star Heat Shield

Fig. 25 Base Pressure Ratio as a Function of Free-Stream Static Pressure, Configuration 1-A

AEDC-TN-61-136

Arnold Engineering Development Center, ARO, Inc., Arnold Air Force Station, Tennessee

AN INVESTIGATION OF BASE HEATING ON A 5.47-PERCENT-SCALE MODEL OF THE SATURN S-1 BOOSTER AT TRANSONIC MACH NUMBERS by T. L. Kennedy and J. F. Lawry, August 1961. 56 pp. (ARO Project No. 224164) (AFSC Program Area 921E, Project 9301) (AEDC-TN-61-136) (Contract No. AF 40(600)-800 S/A 24(61-730)

Unclassified

3 references

An investigation was conducted in the 16-Ft Transonic Tunnel of the Propulsion Wind Tunnel Facility at the Arnold Center to evaluate base heating of the Saturn S-1 booster. Various turbine exhaust stack configurations were tested over a Mach number range of 0.7 to 1.5, an altitude range of 10,000 ft to 42,000 ft, and a missile angle-of-attack range of 0 to +1.2 deg. Rocket engines using liquid oxygen and RP-1 were used to simulate the full-scale

(over)

UNCLASSIFIED

1. Space vehicles--SATURN
2. Space vehicles--Base heating
3. Exhaust gases--Heat transfer
I. Kennedy, T. L.
II. Lawry, J. F.

UNCLASSIFIED

AEDC-TN-61-136

Arnold Engineering Development Center, ARO, Inc., Arnold Air Force Station, Tennessee

AN INVESTIGATION OF BASE HEATING ON A 5.47-PERCENT-SCALE MODEL OF THE SATURN S-1 BOOSTER AT TRANSONIC MACH NUMBERS by T. L. Kennedy and J. F. Lawry, August 1961. 56 pp. (ARO Project No. 224164) (AFSC Program Area 921E, Project 9301) (AEDC-TN-61-136) (Contract No. AF 40(600)-800 S/A 24(61-730)

Unclassified

3 references

An investigation was conducted in the 16-Ft Transonic Tunnel of the Propulsion Wind Tunnel Facility at the Arnold Center to evaluate base heating of the Saturn S-1 booster. Various turbine exhaust stack configurations were tested over a Mach number range of 0.7 to 1.5, an altitude range of 10,000 ft to 42,000 ft, and a missile angle-of-attack range of 0 to +1.2 deg. Rocket engines using liquid oxygen and RP-1 were used to simulate the full-scale

(over)

UNCLASSIFIED

1. Space vehicles--SATURN
2. Space vehicles--Base heating
3. Exhaust gases--Heat transfer
I. Kennedy, T. L.
II. Lawry, J. F.

UNCLASSIFIED

AEDC-TN-61-136

Arnold Engineering Development Center, ARO, Inc., Arnold Air Force Station, Tennessee

AN INVESTIGATION OF BASE HEATING ON A 5.47-PERCENT-SCALE MODEL OF THE SATURN S-1 BOOSTER AT TRANSONIC MACH NUMBERS by T. L. Kennedy and J. F. Lawry, August 1961. 56 pp. (ARO Project No. 224164) (AFSC Program Area 921E, Project 9301) (AEDC-TN-61-136) (Contract No. AF 40(600)-800 S/A 24(61-730)

Unclassified

3 references

An investigation was conducted in the 16-Ft Transonic Tunnel of the Propulsion Wind Tunnel Facility at the Arnold Center to evaluate base heating of the Saturn S-1 booster. Various turbine exhaust stack configurations were tested over a Mach number range of 0.7 to 1.5, an altitude range of 10,000 ft to 42,000 ft, and a missile angle-of-attack range of 0 to +1.2 deg. Rocket engines using liquid oxygen and RP-1 were used to simulate the full-scale

(over)

UNCLASSIFIED

1. Space vehicles--SATURN
2. Space vehicles--Base heating
3. Exhaust gases--Heat transfer
I. Kennedy, T. L.
II. Lawry, J. F.

UNCLASSIFIED

AEDC-TN-61-136

UNCLASSIFIED

AEDC-TN-61-136

UNCLASSIFIED

AEDC-TN-61-136

UNCLASSIFIED

AEDC-TN-61-136

UNCLASSIFIED